A full radius gyrokinetic stability analysis for large aspect ratio finite$-\beta$ tokamaks

R. Ganesh* P. Angelino J. Vaclavik
L. Villard
Centre de Recherches en Physique des Plasmas,
Association EURATOM - Confédération Suisse,
Ecole Polytechnique Fédérale de Lausanne,
1015 Lausanne, Switzerland

October 17, 2003

Abstract

Linear, fully gyrokinetic, full radius (or global), large aspect ratio studies of Alfvén -ion temperature gradient mode (AITG) or Kinetic Ballooning Modes (KBM's) or Beta-induced Alfvén eigenmodes (BAE) considering only "passing" species is presented. Effects hitherto completely neglected in a full radius approach such as $B_{||}-$fluctuations and the ones which have been treated partly[1] such as Shafranov shifts are included. To this end, an existing code EM-GLOGYSTO [1, 2] has been upgraded to incorporate these effects. Among other results, most interesting ones are (i) for relatively large positive magnetic shear $\hat{s}$ ($1.25 < \hat{s} < 4.25, \hat{s} = d\ln q_s/d\ln\rho$, where $q_s(\rho)$ is safety factor and ρ minor radius) $B_{||}$ fluctuations have benign effect on AITG growth rates and for positive but small shear ($0.0 < \hat{s} < 2.7$), $B_{||}$ fluctuations are too weak to play any crucial role (ii) in the later case, inclusion of Shafranov shift leads to the following: (a) growth rates without Shafranov shift effects are in general larger than those including Shafranov shift (b) non-monotonous dependence of growth rates and frequencies on $\beta = 2\mu_0 NT_i/B_0^2$ (c) presence of multiple eigenmodes with competing growth rates for same values of β (d) no sign of complete stabilization with β. Finally eigenmode structures $[\phi, A_{||}, A_{\perp}]$ with and without Shafranov shift are reported. The growth rates and frequencies thus obtained may serve as estimates of transport coefficients and for future bench marking of the (then) global electromagnetic, gyrokinetic, time evolution codes (PIC or otherwise).

*rajaraman.ganesh@epfl.ch

1 Introduction

As tokamak plasmas approach fusion-grade parameters, corresponding increase in plasma β make these machines more and more susceptible to electromagnetic instabilities. In a plasma stable to macroscopic (read system-size) instabilities, free energy in the *gradients* of macroscopic quantities like mean density and temperature give rise to microscale instabilities (read Larmor radius-size) which arise essentially due to particle drifts across magnetic flux surfaces causing transport of particles and energy. In macroscopically stable, low$-\beta$ plasmas, ion temperature gradient (ITG) instabilties are considered as the most dangerous. Present understanding of microscale particle and energy transport is essentially based on ion transport through linear and nonlinear ITG modes regulated by self-generated shear flows (i.e., zonal flows)[3].

On the other hand, particle and energy transport issues connected to electron channel is only beginning to be addressed. One of the logical candidates which has received considerable attention in recent years is electron temperature gradient modes (ETG). Though linear growth rates of these modes are relatively large, a simple mixing length-like estimate fails because of small perpendicular length scale of linear ETG modes. Also, understanding the role of nonlinear ETG modes (i.e., streamers) with their radial finger-like structures and their interaction with zonal flows is an active area of research. Both ITG and ETG based models are predominantly electrostatic. While it is expected that finite$-\beta$ (magnetic) perturbations can have great influence on linear & nonlinear dynamics of electrons and hence can affect their transport, a nontrivial self-consistent model for the origin of these magnetic perturbations and their effect on particle dynamics is still lacking.

Another candidate which is purely electromagnetic (in the sense that it has no zero β counterpart), is Alfvén ion temperature gradient mode (AITG). Physically, one can regard AITGs as arising due to ion compressibility effects on shear Alfvén waves (SAWs) [4, 5, 6, 7, 8] enhanced by electron non-adiabaticity [1] or alternatively they can be understood as a branch connecting kinetic ballooning modes (KBMs) (arising from kinetic effects on MHD ballooning modes) and β induced Alfvén eigenmodes (BAEs) [9]. Importance of AITGs stems from the following: (i) while finite$-\beta$ ITG modes are completely stabilized via its coupling to shear Alfvén waves, AITG becomes more unstable with increasing β values [1, 11]. (ii) as we will see in the next sections, their linear mode structure (i.e., eigenmode width) is inherently mesoscale (occupying a good percent of minor radius) due to drift-induced coupling of flux surfaces and at the same time has a rich microscale structure due to kinetic effects ($E_{||} \neq 0$) such as Landau resonances, ion and electron transit harmonics, kinetic non-adiabaticity and finite Larmor radius (FLR) effects (iii) depending on the magnetic shear values, these modes can couple to $B_{||}-$fluctuations which can in turn have benign effect on AITG growth (iv) they are strongly influenced by Shafranov shift effects: (a) scaling of growth rate with β is substantially

different from (radially) local ballooning calculations [10, 11, 12]; there is no sign of complete stabilization with plasma β, (b) not only are their growth rates affected, their eigenmodes acquire quite a complex radial and poloidal structure; (c) non-monotonic scaling of growth rate and frequency with β; (d) existence of simultaneous multi-mode branches for a given value of β. As a consequence, these flux-surface disrupting, mesoscale (intermediate to Larmor radius and minor radius) magnetic fluctuations ("flutter") thus setup on linear time scale can seriously affect electron transport in quasilinear as well as in nonlinear stages of a full radius "time-evolving" problem. Furthermore, though these modes depend on electron non-adiabaticity (which is enhanced particularly on surfaces with $k_{||} = 0$), the main source of free energy for AITG is still ion-compressibility. Thus, a fully gyrokinetic (FLR effects to all orders), full radius, fully electromagnetic AITG turbulence could be a paradigm which can bridge "ion channel" and "electron channel" of transport through "mesoscale" finite$-\beta$ electromagnetic effects. This paper presents an important step to this above said scenario, namely, a formulation which is linear, non-ballooning (arbitrary 'n', $n-$ toroidal mode number), fully electromagnetic (with both $B_\perp$ and $B_{||}$ fluctuations), fully gyrokinetic (both species), full radius study with Shafranov shift effects (not through the standard '$s-\alpha$' model), parallel resonances, transit harmonics and arbitrary order FLR effects. We will demonstrate many of the above said features of AITGs, some of them perhaps for the first time. Moreover, such a study as ours may serve as a useful bench mark and help gain confidence on nonlinear predictability of (present and future) "time evolving" finite$-\beta$ full radius codes.

In the past there have been a few attempts [13, 14] to develop (electrostatic) global, spectral code in toroidal geometry. Unfortunately, those formulations are only valid up to second order in banana-width and do not take into account any FLR effects. More recently, a full radius study on kinetic MHD modes [15] has been reported. Nevertheless this formulation appears to neglect Shafranov shift effects, which as we will show can dramatically alter the issues at hand. One of the models which partly overcomes the above said problems and computes gyrokinetic growth rate and global eigenmode structures for electrostatic drift waves for both cylinder and torus was developed in Ref.[2, 16]. Later, this model was extended to include low but finite β effects by incorporating parallel vector potential (perpendicular magnetic field) fluctuations in the gyrokinetic equations and parallel component of Ampere's law for current fluctuations. In this model, ions were fully gyrokinetic and electrons were modelled as drift-kinetic [1]. Also in this work, Shafranov shifts effects were shown to be rather "strongly stabilizing" for AITG's or KBM's in the sense that even a small percentage of actual shift [say, 5%] could completely stabilize the mode. Since the reporting of Ref.[1], code EM-GLOGYSTO has been numerically optimized. These numerical improvements will be communicated elsewhere.

The aim of the present work is three-fold : (i) to attempt to generalize the formulation used

in Refs.[1, 2, 16] to incorporate perpendicular vector potential (parallel magnetic field) fluctuations in the gyrokinetic equations and close the system by invoking perpendicular component of Ampere's law[17] (ii) to revisit the Shafranov shift calculations of Ref.[1] such that this effect can be incorporated for parallel and perpendicular B-field fluctuations in a more consistent fashion (iii) to incorporate the above said effects in the code EM-GLOGYSTO and study AITG modes including $B_{||}-$fluctuations and Shafranov shift effects. In the present work, while only fully passing ions and electrons are considered, both species are modelled as gyrokinetic. As we show below, the present model is valid for relatively large β values and wide range of frequencies well above ion temperature gradient modes. Also, the present model contains no trapped particle effects and contains no zeroth order electric field (i.e., equilibrium flows).

In Sec.(2) starting from Vlasov equations, we obtain our basic equation for nonadiabatic part for a given species. Sec.(3) contains definition of gyro-averaging and solution for the nonadiabatic part in "guiding center coordinates" in terms of a propagator, i.e., unit source solution. In Sec.(4) contains the ad-hoc equilibrium used and construction of the propagator in "guiding center coordinates". In Sec.(5) we obtain the relevant physical fluctuating quantities in "particle co-ordinates". Sec.(6) contains the closure of equations and construction of various matrix elements in Fourier space, diagnostics and normalizations used in full radius and local models. Sec.(7) contains derivation of a "local" dispersion from full radius formulation. Sec.(8) contains results and discussions for two sets of equilibrium profiles for studying the effect of $B_{||}$ fluctuation and to study the effect of Shafranov shifts on AITG modes, respectively, followed by some conclusions in Sec.(9) and some possible future direction.

2 Starting Equations

To describe hot toroidal plasmas, collisionless Vlasov-Maxwell equations are used. In the following, we invoke the standard technique of *gyrokinetic* change of variables as employed by P. J. Catto *el al* [18] with *eikonal or spectral ansatz* to obtain a gyrokinetic Vlasov equation. Among others, a self-consistent and energy conserving theoretical framework was provided by T. S. Hahm [19] based on Hamiltonian and Lie transformations and more recently a variational formulation for gyrokinetic Vlasov-Maxwell system was provided by Brizard[20] resulting in gyrokinetic equations and gyro-averaged Maxwell's equations for finite$-\beta$ plasmas. Theoretical formulations used here is an extension of those studied in Ref.[1, 2]. Two major improvements are (i) addition of the $B_{||}$-fluctuation and (ii) appropriate changes in inclusion of Shafranov shift effects.

As appropriate for a linear stability study, the full distribution function $f_j(\mathbf{r}, \mathbf{v}, t)$ of species j is linearized about a suitable equilibrium $f_{0j} = f_{0j}(\mathbf{r}, \mathbf{v})$ such that $f_j(\mathbf{r}, \mathbf{v}, t) = f_{0j}(\mathbf{r}, \mathbf{v}) +$

$f_j(\mathbf{r},\mathbf{v},t)$ with the assumption that $f_j/f_{0j} \ll 1$. Retaining terms up to first order, we get ;

$$\left.\frac{D}{Dt}\right|_{u.t.p.} f_{0j}(\mathbf{r},\mathbf{v}) = 0 \quad \text{where} \quad \left.\frac{D}{Dt}\right|_{u.t.p.} \equiv \frac{\partial}{\partial t} + \mathbf{r}\cdot\nabla + \frac{q_j}{m_j}(\mathbf{v}\times\mathbf{B})\cdot\nabla_{\mathbf{v}} \tag{1}$$

and

$$\left.\frac{D}{Dt}\right|_{u.t.p.} \tilde{f}_j(\mathbf{r},\mathbf{v},t) = -\frac{q_j}{m_j}(\tilde{\mathbf{E}} + \mathbf{v}\times\tilde{\mathbf{B}})\cdot\nabla_{\mathbf{v}} f_{0j} \tag{2}$$

Here $u.t.p$ implies unperturbed trajectories of particles, $\mathbf{B} = B\ \hat{e}_{||}$ is the equilibrium toroidal magnetic field, $\tilde{\mathbf{E}}$ and $\tilde{\mathbf{B}}$ are the perturbed electric and magnetic fields, q_j and m_j are the electric charge and mass of the species respectively. Expressing $\tilde{\mathbf{E}}$ and $\tilde{\mathbf{B}}$ in terms of $\tilde{\varphi}$ and $\tilde{\mathbf{A}}$ and defining the following change of variables $(\mathbf{r},\mathbf{v}) \rightarrow (\mathbf{r}, \xi = v^2/2, \mu = v_\perp^2/2B)$ and using particle canonical angular momentum for species j, i.e., $\psi_{0j} = \hat{e}_\phi \cdot [\mathbf{r}\times(\mathbf{A} + m_j\mathbf{v}/q_j)] = \psi + m_j r v_\phi/q_j$, one can write $f_{0j}(\mathbf{r},\mathbf{v}) = f_{0j}(\mathbf{r},\xi,\mu,\psi_{0j})$. Here cylindrical co-ordinate $\mathbf{r} \equiv (r,\phi,z)$ has been introduced and $\psi = rA_\phi$ is the poloidal flux function per unit radian. Such a transformation would enable one to express f_{0j} in terms of single particle constants of motion. Thus $\nabla_{\mathbf{v}} f_{0j}$ term on $r.h.s$ of Eq.(2) becomes

$$\nabla_{\mathbf{v}} f_{0j}(\mathbf{r},\xi,\mu,\psi_{0j}) = \mathbf{v}\left(1 + \frac{m_j r v_\phi}{q_j}\frac{\partial}{\partial\psi_{0j}}\right)\frac{\partial f_{0j\psi}}{\partial\xi} + \frac{\mathbf{v}_\perp}{B}\frac{\partial f_{0j\psi}}{\partial\mu} + \frac{m_j r\hat{e}_\phi}{q_j}\frac{\partial f_{0j}}{\partial\psi_{0j}}\Bigg|_{\psi_0=\psi} \tag{3}$$

where $f_{0j\psi} \equiv f_{0j}(\psi_{0j} = \psi)$ and $\hat{e}_\phi$ is the toroidal unit vector. To obtain Eq.(3), f_{0j} is Taylor expanded to first order in $\{m_j r v_\phi/q_j\}$ around $\psi_{0j} = \psi$. Then, the following ordering is used :

$$\begin{aligned} &\underline{\text{gyro} - \text{ordering :}} \qquad \frac{\omega}{w_{cj}} \ll 1, \quad k_\perp \varrho_{Lj} \simeq O(1), \quad k_{||}\varrho_{Lj} \simeq \frac{\varrho_{Lj}}{L_{eq}}; \\ &\underline{\text{transport} - \text{ordering :}} \quad \frac{\partial}{\partial\mu} \ll \frac{\partial}{\partial\xi} \end{aligned} \tag{4}$$

where $k_\perp^{-1}, k_{||}^{-1}, \varrho_{Lj}$ are perpendicular and parallel perturbation scales and Larmor radius of the species j respectively and L_{eq} is a typical equilibrium scale length. Rewriting $\tilde{f}_j$ in Eqs.(2), using the change of variables defined by:

$$\tilde{f}_j = h_j^{(0)} + \tilde{\varphi}\frac{q_j}{m_j}\left[\left(1 - \frac{v_\varphi}{\Omega_{pj}}\nabla_n\right)\frac{\partial f_{0j\psi}}{\partial\xi}\right] + \frac{q_j}{m_j B}\frac{\partial f_{0j\psi}}{\partial\mu}\left(\tilde{\varphi} - v_{||}A_{||}\right) - \frac{q_j}{m_j}\frac{A_\phi}{\Omega_{pj}}\nabla_n f_{0j}\Bigg|_{\psi_{0j}=\psi} \tag{5}$$

and then invoking gyro-ordering & transport-ordering followed by some standard vector algebra, we arrive at

$$\left.\frac{D}{Dt}\right|_{u.t.p} h_j^{(0)}(\mathbf{r},\mathbf{v},t) = -\frac{q_j}{m_j}\left[\frac{\partial f_{0j\psi}}{\partial\xi}\frac{\partial}{\partial t} + \frac{v_{||}}{B}\frac{\partial f_{0j\psi}}{\partial\mu}\hat{e}_{||}\cdot\nabla + \frac{1}{\Omega_{pj}}\nabla_n f_{0j}\Bigg|_\psi \hat{e}_\phi\cdot\nabla\right]\left(\tilde{\varphi} - \mathbf{v}\cdot\tilde{\mathbf{A}}\right) + O(\epsilon) \tag{6}$$

In Eqs.(5-6), we have introduced the following definitions: $\Omega_{pj} = w_{cj}B_p/B$, $w_{cj} = q_j B/m_j$, $B_p = |\nabla\psi|/r$ and $h_j^{(0)}$ is the zeroth order term of the perturbative series in the "inverse gyro-frequency expansion" of the nonadiabatic part $h_j = h_j^{(0)} + \frac{1}{w_{cj}}h_j^{(1)} + \frac{1}{w_{cj}^2}h_j^{(2)}$..... Note that since

$D/Dt \simeq O(w_{cj})$, only $h_j^{(0)}$ is retained which is independent of w_{cj} and hence the gyro-angle (defined below). In the rest of this presentation $h_j^{(0)}$ is referred simply as h_j. Eq.(6) is our starting equation.

3 Gyro-Averaging, gauge and solution to the gyrokinetic equation

In a large aspect ratio tokamak geometry, velocity $\mathbf{v}$ of a particle gyrating around a field line is $\mathbf{v} = v_\perp(\hat{e}_\varrho cos\alpha + \hat{e}_\theta sin\alpha) + v_{||}\hat{e}_{||}$, where unit vectors $(\hat{e}_\varrho, \hat{e}_\theta, \hat{e}_\phi)$ define the toroidal co-ordinates and α is the gyro-angle. We define gyro-averaging a quantity "Q" as

$$< Q >= \frac{1}{2\pi}\int_0^{2\pi} d\alpha Q(\alpha; ..)$$

In Eq.(6), the terms in square brackets [..] on the *r.h.s.* are all *equilibrium quantities* and are independent of α. Thus only the potentials are to be averaged. Similarly, on the *l.h.s*, h_j is independent of α, hence, only $D/Dt|_{u.t.p}$ is to be gyro-averaged. Therefore,

$$\left.\frac{D}{Dt}\right|_{u.t.p} \stackrel{gyro-averaging}{\Longrightarrow} \left.\frac{D}{Dt}\right|_{u.t.g} \equiv \frac{\partial}{\partial t} + (v_{||}\hat{e}_{||} + \mathbf{v_{dj}}) \cdot \frac{\partial}{\partial \mathbf{R}}$$

where $\mathbf{v_{dj}} = (v_\perp^2/2 + v_{||}^2)\hat{e}_z/(rw_{cj})$, *u.t.g.* implies *unperturbed trajectory of guiding centers* $\mathbf{R}$ defined by $\mathbf{R} = \mathbf{r} + \mathbf{v} \times \hat{e}_{||}/w_{cj}$. Therefore,

$$< \tilde{\varphi} - \mathbf{v}\cdot\tilde{\mathbf{A}} >= \frac{1}{2\pi}\int_0^{2\pi} d\alpha \left[\ \tilde{\varphi}(\mathbf{r}[\alpha], t) - \mathbf{v}\cdot\tilde{\mathbf{A}}(\mathbf{r}[\alpha], t)\ \right]\Big|_{\mathbf{r}=\mathbf{R}-\mathbf{v}\times\hat{e}_{||}/w_{cj}}$$

Since $\tilde{\varphi}(\mathbf{r}[\alpha], t)$ and $\tilde{\mathbf{A}}(\mathbf{r}[\alpha], t)$ are unknown functions, the gyro-averaging is performed by first Fourier decomposing these functions, then representing the particle co-ordinate $\mathbf{r}$ by gyro-center $\mathbf{R}$ and remembering that

$$J_p(x) = \frac{1}{2\pi}\int_0^{2\pi} d\alpha \exp[\iota(xsin\alpha - p\alpha)]$$

one can obtain a gyro-averaged equation for nonadiabatic distribution function. We choose the following gauge for $\tilde{\mathbf{A}} \equiv (\tilde{A}_{||}, \tilde{A}_\perp) \equiv (\tilde{A}_{||}, \tilde{A}_\theta)$. With the above said procedure, one obtains the following *gyrokinetic equation*:

$$\left.\frac{D}{Dt}\right|_{u.t.g} h_j(\mathbf{R}, \mathbf{v}, t) = -\left(\frac{q_j}{m_j}\right)\left[\frac{\partial f_{0j\psi}}{\partial\xi}\frac{\partial}{\partial t} + \frac{v_{||}}{B}\frac{\partial f_{0j\psi}}{\partial\mu}\hat{e}_{||}\cdot\nabla + \frac{1}{\Omega_{pj}}\nabla_n f_{0j}\Big|_\psi \hat{e}_\phi\cdot\nabla\right]\times$$
$$\left(\tilde{\varphi}(\mathbf{k};)J_0(k_\perp\varrho_{Lj}) - v_{||}\tilde{A}_{||}(\mathbf{k};)J_0(k_\perp\varrho_{Lj}) + \iota\frac{k}{k_\perp}v_\perp\tilde{A}_\theta(\mathbf{k};)J_1(k_\perp\varrho_{Lj})\right) + O(\epsilon) \qquad (7)$$

Solution to Eq.(7) is obtained by *Green function technique* (unit source solution *say* $\mathcal{P}^{sh}$) [21] where *superfix* "sh" indicates that all Shafranov shift effects are contained in $\mathcal{P}^{sh}$. An

explicit form of $\mathcal{P}^{sh}$ is obtained analytically by the method of characteristics of unperturbed trajectories of guiding centers ($u.t.g$) and followed by a perturbative technique for the guiding center velocity [22]. (For a Shafranov circular shifted equilibrium, calculation of $\mathcal{P}^{sh}$ is discussed in the next section). Moreover, the unit source solution, $\mathcal{P}^{sh}$, to Eq.(7) is independent of the type of perturbation (electrostatic or electromagnetic) and solely depends on the considered *equilibrium*. We assume for equilibrium f_{0j}, a local Maxwellian of the form

$$f_{0j}(\xi,\mu,\psi) = f_{Mj}(\xi,\psi) = \frac{N(\psi)}{\left(\frac{2\pi T_j(\psi)}{m_j}\right)^{3/2}}\ \exp -\frac{\xi}{(T_j(\psi)/m_j)}$$

so that $\partial f_{0j}/\partial\mu \equiv 0$ by choice and density profile $N(\psi)$ is independent of the species type j. Thus, for a "sinusoidal" time dependence, the solution to Eq.(7) in guiding center co-ordinates $\mathbf{R}$ is :

$$h_j(\mathbf{R},\mathbf{v},\omega) = -\left(\frac{q_j F_{Mj}}{T_j}\right)\int d\mathbf{k}\exp \imath\mathbf{k}\cdot\mathbf{R}\left(\omega-\omega_j^*\right)\left(\imath\ \mathcal{P}_j^{sh}\right)\times$$
$$\left(\tilde{\varphi}(\mathbf{k};)J_0(k_\perp\varrho_{Lj}) - v_{||}\tilde{A}_{||}(\mathbf{k};)J_0(k_\perp\varrho_{Lj}) + \imath\frac{k}{k_\perp}v_\perp\tilde{A}_\theta(\mathbf{k};)J_1(k_\perp\varrho_{Lj})\right) + O(\epsilon) \tag{8}$$

Here, $\mathbf{k} = \kappa\ \hat{e}_\rho + k_\theta\ \hat{e}_\theta + k_\phi\ \hat{e}_\phi$ and $\kappa = (2\pi/\Delta\rho)\ k_\rho$, with $\Delta\rho = \rho_u - \rho_l$ which defines the radial domain, $k_\phi = n/r$ and $k_\theta = m/\rho$; ω is the *eigenvalue* and $\omega_j^* = \omega_{nj}\left[1+\frac{\eta_j}{2}\left(\frac{v_{||}^2}{v_{thj}^2}-3\right)+\frac{\eta_j v_\perp^2}{2\,v_{thj}^2}\right]$ with $\omega_{nj} = (T_j\nabla_n \ln Nk_\theta)/(q_jB)$ is the *diamagnetic drift frequency*; $\eta_j = (d\ln T_j)/(d\ln N)$. Note also that since the large aspect ratio equilibria considered are axi-symmetric, toroidal mode number "n" can be fixed and the problem is effectively two dimensional in (ρ,θ) (configuration space) or (κ,k_θ) (Fourier space).

4 Ad-hoc equilibrium & propagator construction:

Throughout this work, we will use a Solovev-type magnetic equilibrium of the form $\psi = \psi_0\rho^2/a_0^2$ and in general a circular, non-orthogonal co-ordinates [10] such as

$$r = R_0 + \Delta(\rho) + \rho\ \cos\theta \tag{9}$$
$$z = -\rho\sin\theta \tag{10}$$

such that

$$\frac{\partial\rho}{\partial r} = \frac{\cos\theta}{1+\Delta'(\rho)\cos\theta} \qquad \frac{\partial\rho}{\partial z} = \frac{\sin\theta}{1+\Delta'(\rho)\cos\theta}$$
$$\frac{\partial\theta}{\partial r} = -\frac{\sin\theta}{\rho(1+\Delta'(\rho)\cos\theta)} \qquad \frac{\partial\theta}{\partial z} = \frac{\cos\theta+\Delta'(\rho)}{\rho(1+\Delta'(\rho)\cos\theta)} \tag{11}$$

where R_0 is the major radius, ρ the minor radial co-ordinate, (r,z) represent the cylindrical co-ordinates and $\Delta(\rho)$ the Shafranov shift of circular flux surfaces. It is obvious that such an

equilibrium implies that safety factor profile $q(\rho) = q_0$ should be a constant across the minor radius. Nevertheless, we will study spatially varying q-profiles. In this sense, our configuration space equilibria are rather ad-hoc.

Since a gyro-averaged Vlasov equation can be solved using method of integrating along its *u.t.g*, for our special class of "sinusoidal" time dependence, the unit source solution $\mathcal{P}^{sh}$ is simply

$$\begin{aligned}\mathcal{P}^{sh}(\mathbf{R}, \mathbf{k}, \epsilon, \mu, \sigma, \omega) &= \int_{-\infty}^{t} dt' \exp\left(\iota \left[\mathbf{k} \cdot (\mathbf{R}' - \mathbf{R}) - \omega t'\right]\right) \\ &= \int_{-\infty}^{t} dt' \exp\left(\iota \int^{t'} dt'' \mathbf{k} \cdot \mathbf{v}_g(t'') - \iota \omega t'\right) \end{aligned} \tag{12}$$

where guiding center velocity $d\mathbf{R}/dt = \mathbf{v}_g = \mathbf{v}_{||} + \mathbf{v}_d$ and $\mathbf{R}(t)$ is to be obtained by solving for guiding center trajectories as an "initial value problem" in Shafranov shifted equilibrium considered above. This is done by first assuming that the cross-field drift terms $[\mathbf{v}_d]$ to be small and drop them at the zeroth order and to include them iteratively at the next order. This procedure gives us $\mathcal{P}^{sh}$:

$$\mathcal{P}^{sh} = \sum_{p,p'} \frac{J_p(x_{tj}^{\sigma}) J_{p'}(x_{tj}^{\sigma})}{\omega - \sigma k_{||}^{sh} v_{||} - p\omega_t} \exp(\iota(p - p')(\theta - \bar{\theta}_{\sigma}^{sh})) \tag{13}$$

where $x_{tj}^{\sigma} = k_{\perp}^{sh} \xi_{\sigma}$, $\xi_{\sigma} = v_d/\omega_t, v_d = \left(v_{\perp}^2/2 + v_{||}^2\right)/(\omega_c R), \omega_t = \sigma v_{||}/(q(s)R), \sigma = \pm 1$ (sign of $\mathbf{v}_{||}$) and terms with superfix 'sh' represents those involving Shafranov shift effects. Furthermore $k_{\perp}^{sh} = \sqrt{\kappa^2 + k_{\theta}^2(1 - \Delta'\rho/\xi_{\sigma})^2}$, $k_{||}^{sh} = [nq(s) - m(1 + \xi_{\sigma}\Delta'/(2\rho)]/(q(s)R)$ and $\bar{\theta}_{\sigma}^{sh}$ is defined as $\tan\bar{\theta}_{\sigma}^{sh} = -\kappa/(k_{\theta}(1 - \Delta'\rho/\xi_{\sigma}))$. A few points to be noted here :

- Shafranov shift effects enters the propagator only through $k_{\perp}^{sh}$ and $k_{||}^{sh}$. It is identical to the original propagator in Ref.[2] with various sign dependencies brought out explicitly.
- Shafranov shift dependence on sign of $\mathbf{v}_{||}$ i.e., $\mathbf{v}_{||} = \sigma\ v_{||}$ where $\sigma = \pm 1$ and $v_{||} = |\mathbf{v}_{||}|$
- Argument of transit particle Bessel functions J_p's in Eq.(13) i.e., $x_{tj}^{\sigma} = k_{\perp}^{sh}\xi_{\sigma}$ for $\Delta'(s) \neq 0$ can become $x_{tj} \simeq \mathcal{O}(1)$. Hence transit harmonic orders are to be chosen accordingly.
- While performing the numerical calculations, we have approximated the drift speeds in ξ_{σ} by their local thermal velocity values and hence use $\xi_{\sigma} =< \xi_{\sigma} >= 2\sigma sign(q_j)q(s)\varrho_{Lj}$.

Starting from Grad-Shafranov equation

$$\nabla^2\psi - \frac{2}{r}\frac{\partial\psi}{\partial r} = -\left(I\frac{\partial I}{\partial r} + \mu_0 r^2 \frac{\partial p}{\partial\psi}\right)$$

ordering $\Delta' \simeq \rho$, $I\partial I/\partial r$ and $\partial p/\partial\psi$ to be constants, one can obtain $\psi = \mu_0 j_{\varphi} R\rho^2/4$ and $\Delta' = \rho\partial p/\partial\psi/j_{\varphi}$. Note that the boundary condition $\rho = 0$ at the origin is satisfied through the

explicit dependence on ρ. However, this last expression for Δ' can be expressed first in terms of q(s) and $dp/d\rho$ and introducing the definition of $\beta = 2\mu_0 N T_i/B_\varphi^2$ can be rewritten as

$$\Delta' = \frac{\mu_0}{2} R_0 \frac{dp}{d\rho} \frac{q(s)^2}{B_\varphi^2} \tag{14}$$

For a density profile varying in radial direction, we have

$$\Delta' = -\frac{\beta q^2(s)}{4} \frac{R_0}{a_0} \frac{d\ln N}{ds} \left[(1+\tau) + \eta_i + \tau\eta_e\right] \tag{15}$$

and for a flat density profile, we have

$$\Delta' = -\frac{\beta q^2(s)}{4} \frac{R_0}{a_0} \left[\frac{d\ln T_i}{ds} + \tau \frac{d\ln T_e}{ds}\right] \tag{16}$$

Note that the boundary condition $\Delta'(s=0) = 0$ should now be realized through pressure profiles (density, temperature or both) as the explicit ρ dependence of Δ' has been "used up" in introducing large aspect ratio $q(s)-$profile in the definition of Δ'. In this form $\mathcal{P}^{sh}$ contains effects such as Shafranov shift, transit harmonic and its coupling, parallel velocity resonances and poloidal mode coupling.

5 Fluctuations

To obtain particle density fluctuation $\tilde{n}_j(\mathbf{r};\omega)$ and current densities fluctuations $\tilde{j}_{||}(\mathbf{r};\omega)$ and $\tilde{j}_\theta(\mathbf{r};\omega)$, one needs to go from *g.c.* co-ordinate $\mathbf{R}$ to *particle co-ordinate* $\mathbf{r}$ using $\mathbf{R} = \mathbf{r} + \mathbf{v} \times \hat{e}_{||}/w_{cj}$, by replacing h_j using Eq.(5) followed by the integration over $\mathbf{v}$ keeping in mind the *gyro-angle* integration over α. This last integration on α yields additional Bessel function "J_0" for $\tilde{\varphi}$ and $\tilde{A}_{||}$ whereas it yields "J_1" for $\tilde{A}_\theta$.

Thus, in real space $\mathbf{r}$, for species j, we finally have:

$$\begin{aligned}
\tilde{n}_j(\mathbf{r};\omega) = &-\left(\frac{q_j N}{T_j}\right)\left[\tilde{\varphi} + \int d\mathbf{k}\exp\iota\mathbf{k}\cdot\mathbf{r}\int d\mathbf{v}\frac{f_{Mj}}{N}\left(\omega-\omega_j^*\right)\left(\iota\mathcal{P}_j^{sh}\right)\times\right.\\
&\left.\left\{\left[\tilde{\varphi}(\mathbf{k};) - v_{||}\tilde{A}_{||}(\mathbf{k};)\right]J_0^2(x_{Lj}) + \iota\frac{k}{k_\perp}v_\perp\tilde{A}_\theta(\mathbf{k};)J_0(x_{Lj})J_1(x_{Lj})\right\}\right]\\
\tilde{j}_{||j}(\mathbf{r};\omega) = &-\left(\frac{q_j^2}{T_j}\right)\left[\int d\mathbf{k}\exp\iota\mathbf{k}\cdot\mathbf{r}\int v_{||}d\mathbf{v}f_{Mj}\left(\omega-\omega_j^*\right)\left(\iota\mathcal{P}_j^{sh}\right)\times\right.\\
&\left.\left\{\left[\tilde{\varphi}(\mathbf{k};) - v_{||}\tilde{A}_{||}(\mathbf{k};)\right]J_0^2(x_{Lj}) + \iota\frac{k}{k_\perp}v_\perp\tilde{A}_\theta(\mathbf{k};)J_0(x_{Lj})J_1(x_{Lj})\right\}\right]\\
\tilde{j}_{\theta j}(\mathbf{r};\omega) = &-\left(\frac{q_j^2}{T_j}\right)\left[\int d\mathbf{k}\exp\iota\mathbf{k}\cdot\mathbf{r}\int v_\perp d\mathbf{v}f_{Mj}\left(\omega-\omega_j^*\right)\left(\iota\mathcal{P}_j^{sh}\right)\times\right.\\
&\left.\left\{\iota\frac{k}{k_\perp}\left[\tilde{\varphi}(\mathbf{k};) - v_{||}\tilde{A}_{||}(\mathbf{k};)\right]J_0(x_{Lj})J_1(x_{Lj}) - \frac{k^2}{k_\perp^2}v_\perp\tilde{A}_\theta(\mathbf{k};)J_1^2(x_{Lj})\right\}\right]
\end{aligned} \tag{17}$$

where $x_{Lj} = k_\perp \varrho_{Lj}$. It may be worthwhile to emphasize that "equilibrium effects" such as Shafranov shift (incorporated in $\mathcal{P}^{sh}$) and perturbation effects are clearly delineated in the formulation. Importantly, Shafranov shift parameter ($\Delta'(s)$) appears no where except in $\mathcal{P}^{sh}_j$.

6 Closure and Eigenvalue Matrix

Equations are finally closed by invoking *quasineutrality condition* and Ampere's law.

$$\sum_j \tilde{n}_j(\mathbf{r};\omega) \simeq 0; \qquad \frac{1}{\mu_0}\nabla_\perp^2 \tilde{A}_{||} = -\sum_j \tilde{j}_{||j}; \qquad \frac{1}{\mu_0}\nabla_\perp^2 \tilde{A}_\theta = -\sum_j \tilde{j}_{\theta j} \tag{18}$$

Thus we have 4 (four) unknowns $\omega, \tilde{\varphi}(\mathbf{r}), \tilde{A}_{||}(\mathbf{r}), \tilde{A}_\perp(\mathbf{r})$ and 3 (three) equations Eqs.(18). This eigenvalue problem is conveniently solved in Fourier space. We adopt the following two dimensional Fourier convention:

$$f(\mathbf{k}) = \frac{1}{2\pi}\frac{1}{\Delta\rho}\int_{\rho_l}^{\rho_u} d\rho \int_0^{2\pi} d\theta f(\mathbf{r}) \exp(-\imath\kappa\rho - \imath m\theta) \quad (\text{Fourier} - \text{Transform})$$

$$f(\mathbf{r}) = \int d\mathbf{k} \exp(\imath\mathbf{k}\cdot\mathbf{r}) f(\mathbf{k}) = \sum_{\kappa,m} \exp(\imath\kappa\rho + \imath m\theta) f_{\kappa,m} \quad (\text{Fourier} - \text{Decomposition})$$

where $\Delta\rho = \rho_u - \rho_l$. By Fourier decomposing the potentials in Eq.(18) and then taking Fourier transform,we obtain a convolution matrix in Fourier space. If we assume a hydrogen-like plasma with 2 species (ions and electrons) we have:

$$\sum_{\mathbf{k}'} \begin{pmatrix} \sum_{j=i,e} \hat{\mathcal{M}}^j_{\tilde{\varphi}\tilde{\varphi},\mathbf{k},\mathbf{k}'} & \sum_{j=i,e} \hat{\mathcal{M}}^j_{\tilde{\varphi}\tilde{A}_{||},\mathbf{k},\mathbf{k}'} & \sum_{j=i,e} \hat{\mathcal{M}}^j_{\tilde{\varphi}\tilde{A}_\theta,\mathbf{k},\mathbf{k}'} \\ \sum_{j=i,e} \hat{\mathcal{M}}^j_{\tilde{A}_{||}\tilde{\varphi},\mathbf{k},\mathbf{k}'} & \sum_{j=i,e} \hat{\mathcal{M}}^{j,\nabla^2}_{\tilde{A}_{||}\tilde{A}_{||},\mathbf{k},\mathbf{k}'} & \sum_{j=i,e} \hat{\mathcal{M}}^j_{\tilde{A}_{||}\tilde{A}_\theta,\mathbf{k},\mathbf{k}'} \\ \sum_{j=i,e} \hat{\mathcal{M}}^j_{\tilde{A}_\theta\tilde{\varphi},\mathbf{k},\mathbf{k}'} & \sum_{j=i,e} \hat{\mathcal{M}}^j_{\tilde{A}_\theta\tilde{A}_{||},\mathbf{k},\mathbf{k}'} & \sum_{j=i,e} \hat{\mathcal{M}}^{j,\nabla^2}_{\tilde{A}_\theta\tilde{A}_\theta,\mathbf{k},\mathbf{k}'} \end{pmatrix} \begin{pmatrix} \tilde{\varphi}_{\mathbf{k}'} \\ \tilde{A}_{||,\mathbf{k}'} \\ \tilde{A}_{\theta,\mathbf{k}'} \end{pmatrix} = 0$$

where $\mathbf{k} = (\kappa, m)$ and $\mathbf{k}' = (\kappa', m')$. Numerically, for each species, each of the of these submatrices shown above, is a 2D-band matrix with sub and super diagonals. Note also that the Laplacian for the parallel and perpendicular Ampere's law is added to the appropriate matrix elements above. This matrix is *symmetric* about the diagonal. Hence we write down below the diagonal and upper diagonal elements only. With the following definitions, $\Delta\rho = \rho_u - \rho_l$ (upper and lower radial limits), $\Delta_\kappa = \kappa - \kappa'$ and $\Delta_m = m - m'$ matrix elements are :

$$\hat{\mathcal{M}}^i_{\tilde{\varphi}\tilde{\varphi},\mathbf{k},\mathbf{k}'} = \frac{1}{\Delta\rho}\int_{\rho_l}^{\rho_u} d\rho \exp(-\imath\Delta_\kappa\rho) \times \left[\alpha_p\delta_{mm'} + \exp(\imath\Delta_m\bar{\theta}) \sum_p \hat{I}^0_{p,i}\right]$$

$$\hat{\mathcal{M}}^i_{\tilde{\varphi}\tilde{A}_{||},\mathbf{k},\mathbf{k}'} = -\frac{1}{\Delta\rho}\int_{\rho_l}^{\rho_u} d\rho \exp(-\imath\Delta_\kappa\rho) \times \left[\exp(\imath\Delta_m\bar{\theta}) \sum_p \hat{I}^1_{p,i}\right] \tag{19}$$

$$\hat{\mathcal{M}}^{i}_{\tilde{\varphi}\tilde{A}_\theta,\mathbf{k},\mathbf{k}'} = \frac{1}{\Delta\rho}\int_{\rho_l}^{\rho_u} d\rho\iota\exp(-\iota\Delta_\kappa\rho)\times\frac{\kappa'}{k'_\perp}\left[\exp(\iota\Delta_m\bar{\theta})\sum_p \hat{V}^0_{p,i}\right]$$

$$\hat{\mathcal{M}}^{e}_{\tilde{\varphi}\tilde{\varphi},\mathbf{k},\mathbf{k}'} = \frac{1}{\Delta\rho}\int_{\rho_l}^{\rho_u} d\rho\exp(-\iota\Delta_\kappa\rho)\times\left[\frac{\alpha_p}{\tau(\rho)}\delta_{mm'}+\frac{\exp(\iota\Delta_m\bar{\theta})}{\tau(\rho)}\sum_p \hat{I}^0_{p,e}\right]$$

$$\hat{\mathcal{M}}^{e}_{\tilde{\varphi}\tilde{A}_{||},\mathbf{k},\mathbf{k}'} = -\frac{1}{\Delta\rho}\int_{\rho_l}^{\rho_u} d\rho\exp(-\iota\Delta_\kappa\rho)\times\left[\frac{\exp(\iota\Delta_m\bar{\theta})}{\tau(\rho)}\sum_p \hat{I}^1_{p,e}\right]$$

$$\hat{\mathcal{M}}^{e}_{\tilde{\varphi}\tilde{A}_\theta,\mathbf{k},\mathbf{k}'} = \frac{1}{\Delta\rho}\int_{\rho_l}^{\rho_u} d\rho\exp(-\iota\Delta_\kappa\rho)\times\frac{\kappa'}{k'_\perp}\left[\frac{\iota\exp(\iota\Delta_m\bar{\theta})}{\tau(\rho)}\sum_p \hat{V}^0_{p,e}\right]$$

Since $\hat{\mathcal{M}}^{i,\nabla^2}_{\tilde{A}_{||}\tilde{A}_{||},\mathbf{k},\mathbf{k}'} = \hat{\mathcal{M}}^{i}_{\tilde{A}_{||}\tilde{A}_{||},\mathbf{k},\mathbf{k}'} + \hat{\mathcal{M}}^{\nabla^2}_{\tilde{A}_{||}\tilde{A}_{||},\mathbf{k},\mathbf{k}'}$ we have

$$\hat{\mathcal{M}}^{i}_{\tilde{A}_{||}\tilde{A}_{||},\mathbf{k},\mathbf{k}'} = \frac{1}{\Delta\rho}\int_{\rho_l}^{\rho_u} d\rho\exp(-\iota\Delta_\kappa\rho)\times\left[\exp(\iota\Delta_m\bar{\theta})\sum_p \hat{I}^2_{p,i}\right] \tag{20}$$

$$\hat{\mathcal{M}}^{\nabla^2}_{\tilde{A}_{||}\tilde{A}_{||},\mathbf{k},\mathbf{k}'} = -\frac{1}{\Delta\rho}\int_{\rho_l}^{\rho_u} d\rho\exp(-\iota\Delta_\kappa\rho)\left(\kappa'^2+\frac{m'^2}{\rho^2}\right)\left(\frac{T_i(\rho)}{q_i^2 N\mu_0}\right)$$

$$\hat{\mathcal{M}}^{e}_{\tilde{A}_{||}\tilde{A}_{||},\mathbf{k},\mathbf{k}'} = \frac{1}{\Delta\rho}\int_{\rho_l}^{\rho_u} d\rho\frac{\exp(-\iota\Delta_\kappa\rho)}{\tau(\rho)}\times\left[\exp(\iota\Delta_m\bar{\theta})\sum_p \hat{I}^2_{p,e}\right]$$

$$\hat{\mathcal{M}}^{i}_{\tilde{A}_{||}\tilde{A}_\theta,\mathbf{k},\mathbf{k}'} = -\frac{1}{\Delta\rho}\int_{\rho_l}^{\rho_u} d\rho\iota\exp(-\iota\Delta_\kappa\rho)\times\frac{\kappa'}{k'_\perp}\left[\exp(\iota\Delta_m\bar{\theta})\sum_p \hat{V}^1_{p,i}\right]$$

$$\hat{\mathcal{M}}^{e}_{\tilde{A}_{||}\tilde{A}_\theta,\mathbf{k},\mathbf{k}'} = -\frac{1}{\Delta\rho}\int_{\rho_l}^{\rho_u} d\rho\frac{\iota}{\tau(\rho)}\exp(-\iota\Delta_\kappa\rho)\times\frac{\kappa'}{k_{\perp'}}\left[\exp(\iota\Delta_m\bar{\theta})\sum_p \hat{V}^1_{p,e}\right]$$

Since $\hat{\mathcal{M}}^{i,\nabla^2}_{\tilde{A}_\theta\tilde{A}_\theta,\mathbf{k},\mathbf{k}'} = \hat{\mathcal{M}}^{i}_{\tilde{A}_\theta\tilde{A}_\theta,\mathbf{k},\mathbf{k}'} + \hat{\mathcal{M}}^{\nabla^2}_{\tilde{A}_\theta\tilde{A}_\theta,\mathbf{k},\mathbf{k}'}$ we have

$$\hat{\mathcal{M}}^{i}_{\tilde{A}_\theta\tilde{A}_\theta,\mathbf{k},\mathbf{k}'} = -\frac{1}{\Delta\rho}\int_{\rho_l}^{\rho_u} d\rho\exp(-\iota\Delta_\kappa\rho)\times\frac{\kappa'^2}{k^2_{\perp'}}\left[\exp(\iota\Delta_m\bar{\theta})\sum_p \hat{W}^0_{p,i}\right]$$

$$\hat{\mathcal{M}}^{e}_{\tilde{A}_\theta\tilde{A}_\theta,\mathbf{k},\mathbf{k}'} = -\frac{1}{\Delta\rho}\int_{\rho_l}^{\rho_u} d\rho\exp(-\iota\Delta_\kappa\rho)\times\frac{\kappa'^2}{k^2_{\perp'}}\left[\frac{\exp(\iota\Delta_m\bar{\theta})}{\tau(\rho)}\sum_p \hat{W}^0_{p,e}\right] \quad \text{where}$$

$$\hat{I}^l_{p,j} = \frac{1}{\sqrt{2\pi}v^3_{th,j}(\rho)}\int_{-vmax_j(\rho)}^{vmax_j(\rho)} v^l_{||}dv_{||}\exp-\left(\frac{v^2_{||}}{v^2_{th,j}(\rho)}\right)\left\{\frac{N^j_1 I^\sigma_{0,j}-N^j_2 I^\sigma_{1,j}}{D^{\sigma,j}_1}\right\}_{p'=p-(m-m')}$$

$$\hat{V}^l_{p,j} = \frac{1}{\sqrt{2\pi}v^3_{th,j}(\rho)}\int_{-vmax_j(\rho)}^{vmax_j(\rho)} v^l_{||}dv_{||}\exp-\left(\frac{v^2_{||}}{v^2_{th,j}(\rho)}\right)\left\{\frac{N^j_1 V^\sigma_{0,j}-N^j_2 V^\sigma_{1,j}}{D^{\sigma,j}_1}\right\}_{p'=p-(m-m')} \tag{21}$$

$$\hat{W}^l_{p,j} = \frac{1}{\sqrt{2\pi}v^3_{th,j}(\rho)}\int_{-vmax_j(\rho)}^{vmax_j(\rho)} v^l_{||}dv_{||}\exp-\left(\frac{v^2_{||}}{v^2_{th,j}(\rho)}\right)\left\{\frac{N^j_1 W^\sigma_{0,j}-N^j_2 W^\sigma_{1,j}}{D^{\sigma,j}_1}\right\}_{p'=p-(m-m')}$$

and

$$I^\sigma_{n,j} = \int_{-v_{\perp max,j(\rho)}}^{v_{\perp max,j(\rho)}} v^{2n+1}_\perp dv_\perp\exp-\left(\frac{v^2_\perp}{2v^2_{th,j}(\rho)}\right)J^2_0(x_{Lj})J_p(x'^\sigma_{tj})J_{p'}(x'^\sigma_{tj})$$

$$V^{\sigma}_{n,j} = \int_{-v_{\perp max,j(\rho)}}^{v_{\perp max,j(\rho)}} v_{\perp}^{2n+2} dv_{\perp} \exp - \left(\frac{v_{\perp}^2}{2v_{th,j}^2(\rho)}\right) J_0(x_{Lj}) J_1(x_{Lj}) J_p(x'^{\sigma}_{tj}) J_{p'}(x'^{\sigma}_{tj}) \qquad (22)$$

$$W^{\sigma}_{n,j} = \int_{-v_{\perp max,j(\rho)}}^{v_{\perp max,j(\rho)}} v_{\perp}^{2n+3} dv_{\perp} \exp - \left(\frac{v_{\perp}^2}{2v_{th,j}^2(\rho)}\right) J_1^2(x_{Lj}) J_p(x'^{\sigma}_{tj}) J_{p'}(x'^{\sigma}_{tj})$$

We have introduced the following definitions: $v_{\perp max,j(\rho)} = min(v_{||}/\sqrt{\epsilon}, v_{max,j})$ which is "trapped particle exclusion" from ω independent perpendicular velocity integrals namely, $I^{\sigma}_{n,j}$, $V^{\sigma}_{n,j}$, $W^{\sigma}_{n,j}$; $\alpha_p = 1 - \sqrt{\epsilon/(1+\epsilon)}$ is the fraction of passing particles; $\hat{I}^{l}_{p,j}$, $\hat{W}^{l}_{p,j}$, $\hat{V}^{l}_{p,j}$ are $\omega-$dependent parallel integrals; $x^{\sigma}_{tj} = k^{sh}_{\perp}\xi_{\sigma}$, $N^{j}_{1} = \omega - w_{n,j}\left[1 + (\eta_j/2)(v^2_{||}/v^2_{th,j}) - 3)\right]$; $N^{j}_{2} = w_{n,j}\eta_j/(2v^2_{th,j})$ and $D^{\sigma,j}_{1} = < w_{t,j}(\rho) > (nq_s - m'(1+\xi_{\sigma}\Delta'/(2\rho) - p)(\sigma v_{||}/v_{th,j}) - \omega$ where $< w_{t,j}(\rho) >= v_{th,j}(\rho)/(rq_s)$ is the average *transit frequency* of the species j. As Eqs.(22) are independent of ω and dependent only on $v_{\perp}$, σ and other equilibrium quantities, one may choose to calculate and store them as interpolation tables (memory intensive) or alternatively, one may choose to calculate them when needed (CPU-time intensive). We would like to point out a few useful and simplifying assumptions used in the numerical implementation of velocity integrals described above: (a) We have used a flux surface averaged passing particle fraction α_p correct up to first order in inverse aspect ratio ϵ. Hence we have, for trapped particle exclusion $v_{\perp} < v_{||}/\sqrt{\epsilon}$. If one were to use a general expression (i.e., not averaged over flux surface and correct up to arbitrary order in ϵ), then $\alpha_p = 1 - \sqrt{\epsilon(1+\cos\theta)/(1+\epsilon\cos\theta)}$. Our simplification eliminates additional complication that would result out of θ coupling in the limits of velocity integrals in our 2-dimensional full radius approach. Alternatively, one may either use a first order (in ϵ) "outboard side ($\theta = 0$)" estimate with $\alpha_p = 1 - \sqrt{2\epsilon/(1+\epsilon)}$ and $v_{\perp} < v_{||}/\sqrt{2\epsilon}$ or use a $\theta-$independent empirical fit for $\alpha_p = \alpha_p(\epsilon)$. (b) To be consistent with assumption-(a) used in computing nonadiabatic contributions, the adiabatic response is then multiplied by an appropriate passing particle fraction. While these assumption may over-estimate (or under-estimate) the responses by certain margin, we believe that, in general, they do not affect the nature of our results. More over, absence of trapped particles for the present model allows some leverage on velocity-space boundaries. (c) In Eqs.(20), nonadiabatic electron contribution to electrostatic component of $\hat{\mathcal{M}}^{e}_{\tilde{\varphi}\tilde{\varphi},\mathbf{k},\mathbf{k}'}$ is neglected. (d) Various numerical convergence tests have been performed with number of radial and poloidal Fourier modes, equilibrium profile discretization and velocity integrals. In the next section, we will specify some diagnostics and normalizations used in the code.

6.1 Diagnostics : Eigenmode-averaged quantities

As simple extension of diagnostics discussed in Ref.[1, 2] one can include the contribution from the third component A_{θ} ($B_{||}-$fluctuations) to various physical quantities such as k_{ρ}, k_{θ} as

averages over the eigenmode:

$$< k_\rho^2 >= \frac{\sum_{(k,m)} |\kappa\varphi_{(k,m)}|^2 + |\kappa A_{||(k,m)}|^2 + |\kappa A_{\theta(k,m)}|^2)}{\sum_{(k,m)} |\varphi_{(k,m)}|^2 + |A_{||(k,m)}|^2 + |A_{\theta(k,m)}|^2}$$

$$< k_\theta >= \frac{\int d\rho \sum_m |\frac{m}{\rho}\varphi_{(k,m)}|^2 + \int d\rho \sum_m |\frac{m}{\rho} A_{||(k,m)}|^2 + \int d\rho \sum_m |\frac{m}{\rho} A_{\theta(k,m)}|^2}{\int d\rho \sum_m |\varphi_{(k,m)}|^2 + \int d\rho \sum_m |A_{||(k,m)}|^2 + \int d\rho \sum_m |A_{\theta(k,m)}|^2} \quad (23)$$

Similarly, a simple diagnostic for measuring the electromagnetic ratio is defined as:

$$\frac{< A_{||}^2 >}{< \varphi^2 >} = \frac{\sum_{(k,m)} |A_{||(k,m)}|^2}{\sum_{(k,m)} |\varphi_{(k,m)}|^2}$$

$$\frac{< A_\theta^2 >}{< \varphi^2 >} = \frac{\sum_{(k,m)} |A_{\theta(k,m)}|^2}{\sum_{(k,m)} |\varphi_{(k,m)}|^2} \quad (24)$$

where quantities with suffix "(k, m)" imply Fourier weights of corresponding perturbations.

6.2 Normalization for full radius calculation

Distances are normalized to minor radius "a"; i.e., $s = \rho/a$. Radial position where η_j peaks is represented as $s = s_0$. Frequencies and growth rates are normalized to $\omega_{d0} = v_{thi}(s = s_0)\varrho_{Li}/a^2$, $k_\perp$ is normalized to its local (ion/electron) Larmor radius $\varrho_{Lj}(s)$, $k_{||}$ to L_n (density gradient length scale), $[A_{||}, A_\perp]$ to $v_{thi}(s = 0)$, magnetic field B to $B(s = 0)$, density to $N(s = s_0)$, temperature T to $T(s = s_0)$, velocities $(v_\perp, v_{||})$ to $v_{thi}(s)$ (i.e., to their radially local thermal values).

All input quantities to the code are in SI units, except temperature of given species which is in eV. Hence for example, v_{thi} is computed using $v_{thi}^2(\text{in } m/s) = T_i(\text{in Joule})/m_i(\text{in Kg}) = |e|T_i(\text{in eV})/m_i(\text{in Kg})$ where $|e|$ is absolute value of electronic charge. Similarly, plasma density get defined through (*input*) plasma β at $s = s_0$ i.e., $N(s_0) = (\beta(s_0)B^2(s = 0)/(2\mu_0|e|)) \times 1/(T_i(eV) + T_e(eV))$. Thus, for example, for parameters throughout this work(Sec.8 to follow), we have $\omega_{d0} \simeq 3 \times 10^4\ Hz$. Also, note that for given ion and electron temperature profiles, scaling β amounts to scaling density value at $s = s_0$.

6.3 Normalization for the local calculation

Values for safety factor (q) and the radial location where growth rates are to be computed using local dispersion is chosen from the average mode location obtained from full radius calculation. Frequencies are normalized to v_{thj}/L_n where L_n is the density gradient length scale; thus $\omega_{d0}[\text{full radius}] = \omega_{d0}[\text{local}] \times \frac{\varrho_{Lj} L_n}{a^2}$. Again, $k_\perp$ is normalized to ϱ_{Lj}, $k_{||} = 1/(qR)$ (connection length). Velocity space normalizations are same as for the full radius calculation.

7 Local Gyrokinetic Dispersion : Only passing particles

Before attempting any solution to the full radius equations [Eqs.(18)-(22)], we solve a much simplified local dispersion (at a radial point $s_0 = \rho_0/a$ for a given $\mathbf{k}$) for the case without Shafranov shift ($\Delta' = 0$) but with all 3 potentials viz $[\varphi_{\mathbf{k}}, A_{||,\mathbf{k}}, A_{\perp,\mathbf{k}}]$ with a choice of gauge convenient for local calculations ($k_\theta/k_\perp \simeq 1$) namely $A_{\perp,\mathbf{k}} = (A_{\rho,\mathbf{k}}, A_{\theta,\mathbf{k}}) = A_{\rho,\mathbf{k}}$. Note that if one calculates local dispersion with $A_{\theta,\mathbf{k}} \equiv 0$, one gets the same equations [as shown below] with $k_\theta/k_\perp$ replaced by $\kappa/k_\perp$. Let us represent the propagator $\mathcal{P}_j^{sh}$ as $\mathcal{P}_{local}$, suppresing the species indices "j" and "sh". Since there are no radial excursions allowed in a "local" analysis, the drift velocity $\mathbf{v}_d$ would now be independent of "time" (see Eq.12) and hence the propagator is simply

$$\iota\mathcal{P}_{local} = -\frac{1}{\omega - k_{||}v_{||} - \mathbf{k}\cdot\mathbf{v}_d} \tag{25}$$

Note that there is no straightforward way of recovering Eq.(25) from Eq.(13). Now, in Eq.(18) considering a single wave vector $\mathbf{k}$ and substituting Eq.(25) for $\mathcal{P}_j^{sh} = \mathcal{P}_{local}$ with gauge $A_\perp = A_\rho$ we get

$$\tilde{n}_{j,\mathbf{k}}(\omega) = -\left(\frac{q_j N}{T_j}\right)\left[\tilde{\varphi}(\mathbf{k}) + \int d\mathbf{v}\frac{f_{Mj}}{N}\left(\omega - \omega_j^*\right)(\iota\mathcal{P}_{local}) \times \right.$$
$$\left.\left\{\left[\tilde{\varphi}(\mathbf{k};) - v_{||}\tilde{A}_{||}(\mathbf{k};)\right]J_0^2(x_{Lj}) + \iota\frac{k}{k_\perp}v_\perp\tilde{A}_\rho(\mathbf{k};)J_0(x_{Lj})J_1(x_{Lj})\right\}\right]$$
$$\tilde{j}_{||j,\mathbf{k}}(\omega) = -\left(\frac{q_j^2}{T_j}\right)\left[\int v_{||}d\mathbf{v}f_{Mj}\left(\omega - \omega_j^*\right)(\iota\mathcal{P}_{local}) \times \right.$$
$$\left.\left\{\left[\tilde{\varphi}(\mathbf{k};) - v_{||}\tilde{A}_{||}(\mathbf{k};)\right]J_0^2(x_{Lj}) + \iota\frac{k}{k_\perp}v_\perp\tilde{A}_\rho(\mathbf{k};)J_0(x_{Lj})J_1(x_{Lj})\right\}\right] \tag{26}$$
$$\tilde{j}_{\rho j,\mathbf{k}}(\omega) = -\left(\frac{q_j^2}{T_j}\right)\left[\int v_\perp d\mathbf{v}f_{Mj}\left(\omega - \omega_j^*\right)(\iota\mathcal{P}_{local}) \times \right.$$
$$\left.\left\{\iota\frac{k}{k_\perp}\left[\tilde{\varphi}(\mathbf{k};) - v_{||}\tilde{A}_{||}(\mathbf{k};)\right]J_0(x_{Lj})J_1(x_{Lj}) - \frac{k^2}{k_\perp^2}v_\perp\tilde{A}_\rho(\mathbf{k};)J_1^2(x_{Lj})\right\}\right]$$

where $x_{Lj} = k_\perp\varrho_{Lj}$. Using quasi-neutrality (or Poisson equation), parallel and perpendicular Ampere's law to close the system of equations results in the following set of algebraic equations *viz.*,

$$\left[k_\perp^2\lambda_{Di}^2\tau + (1+\tau) - \tau\tilde{I}_{0,0}^i - \tilde{I}_{0,0}^e\right]\tilde{\varphi}(\mathbf{k}) + \left[v_{thi}\tau\tilde{I}_{1,0}^i + v_{the}\tilde{I}_{1,0}^e\right]\tilde{A}_{||}(\mathbf{k}) + \iota\left[v_{thi}\tau\tilde{V}_{0,1}^i + v_{the}\tilde{V}_{0,1}^e\right]\tilde{A}_\rho(\mathbf{k}) = 0$$

(A_1) (A_2) (A_3)

$$\left[v_{thi}\tau\tilde{I}^{i}_{1,0}+v_{the}\tilde{I}^{e}_{1,0}\right]\tilde{\varphi}(\mathbf{k})-\left[\frac{k_{\perp}^{2}T_{i}}{\mu_{0}Nq^{2}}\tau+v^{2}_{thi}\tau\tilde{I}^{i}_{2,0}+v^{2}_{the}\tilde{I}^{e}_{2,0}\right]\tilde{A}_{||}(\mathbf{k})-\iota\left[v^{2}_{thi}\tau\tilde{V}^{i}_{1,1}+v^{2}_{the}\tilde{V}^{e}_{1,1}\right]\tilde{A}_{\rho}(\mathbf{k})=0$$

(B_1) (B_2) (B_3)

$$\iota\left[v_{thi}\tau\tilde{V}^{i}_{0,1}+v_{the}\tilde{V}^{e}_{0,1}\right]\tilde{\varphi}(\mathbf{k})-\iota\left[v^{2}_{thi}\tau\tilde{V}^{i}_{1,1}+v^{2}_{the}\tilde{V}^{e}_{1,1}\right]\tilde{A}_{||}(\mathbf{k})+\left[\frac{k_{\perp}^{2}T_{i}}{\mu_{0}Nq^{2}}\tau+v^{2}_{thi}\tau\tilde{W}^{i}_{0,2}+v^{2}_{the}\tilde{W}^{e}_{0,2}\right]\tilde{A}_{\rho}(\mathbf{k})=0$$

(C_1) (C_2) (C_3)

Here the dispersion relation obtained when the determinant of the above given "matrix" is set to zero. Note that "matrix" is symmetric about the diagonal i.e., $B_1 \equiv A_2,\ C_1 \equiv A_3,\ C_2 \equiv B_3$ hence dispersion relation is

$$\left[A_1B_2-A_2^2\right]C_3+2\,A_2A_3B_3-A_1B_3^2-A_3^2B_2=0 \tag{27}$$

In the above "matrix", the velocity integrals are defined as follows:

$$\begin{aligned}\tilde{I}^{j}_{l,p}&=\mathcal{Q}\odot\left(\frac{v_{||}}{v_{thj}}\right)^{l}\left(\frac{v_{\perp}}{v_{thj}}\right)^{p}J_0^2(x_{Lj})\\ \tilde{V}^{j}_{l,p}&=\mathcal{Q}\odot\left(\frac{v_{||}}{v_{thj}}\right)^{l}\left(\frac{v_{\perp}}{v_{thj}}\right)^{p}J_0(x_{Lj})J_1(x_{Lj})\\ \tilde{W}^{j}_{l,p}&=\mathcal{Q}\odot\left(\frac{v_{||}}{v_{thj}}\right)^{l}\left(\frac{v_{\perp}}{v_{thj}}\right)^{p}J_1^2(x_{Lj})\end{aligned} \tag{28}$$

where

$$\mathcal{Q}\equiv\frac{1}{\sqrt{2\pi}}\int\left(\frac{v_{\perp}dv_{\perp}dv_{||}}{v^{3}_{thj}}\right)\exp\left(-\frac{v^{2}}{2v^{2}_{thj}}\right)\frac{\left(\omega-\omega^{*}_{j}\right)}{\left(\omega-k_{||}v_{||}-\omega_{dj}\right)} \tag{29}$$

and the symbol $\odot$ reminds us that $\mathcal{Q}$ is an integral operator. In the "matrix" defined above, $k_\perp$ is the perpendicular wave vector, λ_{Di} is the ion Debye length scale, $\tau = T_e/T_i$ is the ratio of electron to ion temperatures, $v_{thi,e}$ is thermal speeds of ion/electron, μ_0 is the permittivity of free space, $N-$ density (same for both species) and q^2 is square of the electronic charge. One can recover the "electrostatic" gyrokinetic ITG/ETG dispersion[23] by setting $A2, A_3, B_3 \equiv 0$ (B_2, C_3- indeterminate), i.e.,

$$\left[k_{\perp}^{2}\lambda^{2}_{Di}\tau+(1+\tau)-\tau\tilde{I}^{i}_{0,0}-\tilde{I}^{e}_{0,0}\right]=0$$

This above equation yields critical η_j i.e., $\eta_{c,j} \geq 2/3$ if all other species except "j" are assumed to be adiabatic in nature. Similarly, low$-\beta$ "electromagnetic" gyrokinetic (A)ITG/ETG dispersion [1] is obtained by setting $A_3, B_3 \equiv 0$ (C_3 is indeterminate) i.e.,

$$\left[k_{\perp}^{2}\lambda^{2}_{Di}\tau+(1+\tau)-\tau\tilde{I}^{i}_{0,0}-\tilde{I}^{e}_{0,0}\right]\times\left[\frac{k_{\perp}^{2}T_{i}}{\mu_{0}Nq^{2}}\tau+v^{2}_{thi}\tau\tilde{I}^{i}_{2,0}+v^{2}_{the}\tilde{I}^{e}_{2,0}\right]+\left[v_{thi}\tau\tilde{I}^{i}_{1,0}+v_{the}\tilde{I}^{e}_{1,0}\right]^{2}=0$$

Finally, one can obtain "magnetostatic" gyrokinetic mode by setting all elements except C_3 to zero, i.e.,

$$\left[\frac{k_\perp^2 T_i}{\mu_0 N q^2}\tau + v_{thi}^2 \tau \tilde{W}_{0,2}^i + v_{the}^2 \tilde{W}_{0,2}^e\right] = 0$$

In the sections to follow, for purposes of comparision with full radius calculations, Eq.(27) along with Eq.(28) and Eq.(29) are solved numerically at a given radial location $s_0 = \rho/a$ and for various values of β. Also note that, from the "matrix" defined above Eq.(27), one can compute the electromagnetic ratio (E.M. ratio) such as $(v_{th}A_{||}/\varphi)^2$, $(v_{th}A_\perp/\varphi)^2$ evaluated at the root of the determinant Eq.(27) i.e, at the eigenvalue, say, $\omega_0 = \gamma + \iota\omega_r$. Hence,

$$\left[\frac{v_{th}\ \tilde{A}_{||}}{\tilde{\varphi}}\right]^2_{\omega_0} = \left[\frac{B_3C_1 - B_1C_3}{B_2C_3 - C_2^2}\right]^2_{\omega_0}\ ; \qquad \left[\frac{v_{th}\ \tilde{A}_{\perp}}{\tilde{\varphi}}\right]^2_{\omega_0} = \left[\frac{B_1C_2 - B_2C_1}{B_2C_3 - C_2^2}\right]^2_{\omega_0} \tag{32}$$

It may be worthwhile to emphasize that Eq.(27) along with Eq.(28) and Eq.(29) is the most general dispersion relation within the assumptions made.

8 Results & Discussion

To bring out some of the salient features of our full radius formulation with $B_{||}-$ field fluctuations and Shafranov shift effects, we have chosen two sets of "equilibrium" profiles, both these profiles are "ad-hoc" in the sense that $q-$profiles vary in space and hence the shear profiles too, whereas, as pointed out before, our choice of "Solovev"-type flux-function $\psi/\psi_0 = \rho^2/a^2$ implies $q(s = \rho/a) = const.$

8.1 $B_{||}$ stabilization of AITG's without Shafranov shift

In this section, we solve the full two dimensional (ρ, θ) or (κ, k_θ) fully gyrokinetic, fully electromagnetic equations with 3 potentials *viz.,* $[\varphi, A_{||}, A_\perp]$ considering only passing species and neglecting Shafranov shift effects (i.e., $\Delta'(\rho) = 0$ through out). Consider the following parameters and profiles:

Parameters-I:

- B-field : $B_0 = 1.0$ Tesla
- Temperature : $T_0 = T(s0) = 7.5\ KeV$
- Major Radius : $R = 2.0\ m$
- Minor Radius : $a = 0.5\ m$
- radius : $s = \rho/a\ \ 0.1 < s < 1.0$
- $\beta(s_0) = \frac{2\mu_0 N_0}{B_0^2}(T_0^e + T_0^i)$ defines N_0
- $L_{n0} = 0.4,\ L_{T0} = 0.2\ m \rightarrow \eta(s_0) = 2.0$
- $\tau(s) = T^e(s)/T^i(s) = 1$ throughout.

Equilibrium Profiles-I:

- N-profile and T-profile

$N(s)/N_0 = \exp\left(-\frac{a\,\delta s_n}{L_{n0}}\ \tanh\left(\frac{s-s_0}{\delta s_n}\right)\right)$

$T(s)/T_0 = \exp\left(-\frac{a\,\delta s_T}{L_{T0}}\ \tanh\left(\frac{s-s_0}{\delta s_T}\right)\right)$

$\delta s_n = 0.35,\ \delta s_T = 0.2$ at $s = s_0$

- q-profile & $\hat{s}$-profile:

$q(s) = 1.25 + 0.67\ s^2 + 2.38\ s^3 - 0.06\ s^4$

such that $q(s = s_0) = 2.0$;

Shear $\hat{s}$ is positive and at $s = s_0,\ \hat{s} = 1.$

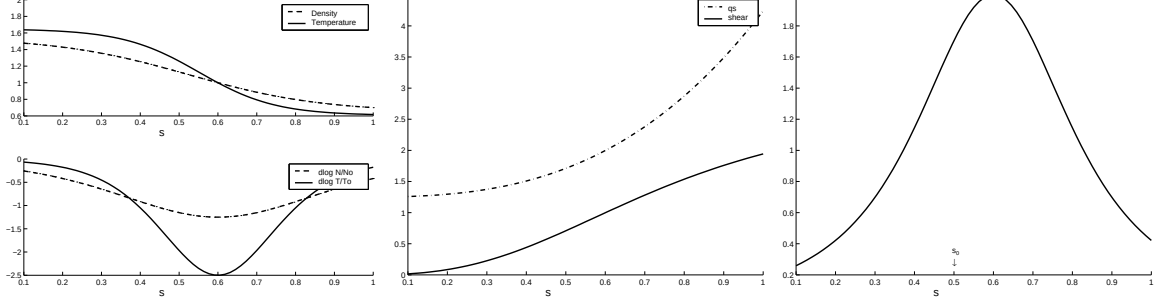

Figure 1: *Equilibrium profiles - I for $B_{||}$ stabilization with $\Delta'(\rho) = 0$*

For these parameters equibrium profiles are shown in Fig.1 while normalized growth rates and real frequencies as functions of plasma β are represented in Fig.2. In Fig.(2 a,b) note that the results of local dispersion analysis of Sec.(7) and the full radius results show very different behaviour as a function of β. Not only are there quantitative differences, there are sharp qualitative differences: (i) for $\beta > 4\%$, local 3-potential $[\tilde{\varphi}, \tilde{A}_{||}, \tilde{A}_{\perp}]$ calculations [open circles] and full radius 3-potential calculations [filled circles] predict opposite tendenies for growth rates as function of β: while full radius calculations predict that $B_{||}$ fluctuations have stabilizing tendency with β on AITG, the local results predict an initial fall and then increase in growth rate after $\beta \simeq 10\%$ (ii) while real frequencies from 3 potential local calculations [see inset Fig.(2b)] show that for $\beta < 10\%$, AITG's rotate in "ion diamagnetic" direction and for $\beta > 10\%$, they rotate in "electron diamagnetic" direction; where as full radius calculations show non-monotonic behaviour of ω/ω_{d0} with β and never cross $\omega/\omega_{d0} = 0$ line. Similarly, a comparision with 2 potential $[\varphi, A_{||}]$ full radius [filled diamonds] calculations and 3 potential $[\varphi, A_{||}, A_{\perp}]$ full radius [filled circles] shows the following: (i) $B_{||}$ fluctuations begin to have any effect at all on AITGs only for $\beta > 7\%$. (ii) for $\beta > 10\%$, while 3 potential calculations show steady decrease in growth rate with increasing β, where as 2 potential results show continous increase; consequently in the absence of Shafranov shift effects and for postive large shear values, $B_{||}-$fluctuations have benign effect on AITG's. (iii) while real frequencies in both cases are non-monotonic, 2 potential calculations show that for large β, AITG would rotate more in ion diagmagnetic direction where as 3 potential calculations show opposite tendency.

To compare the local calculations with 2 potential [open diamonds] and 3 potential [open circles] calculations [see insets Fig.(2a,b)]: (i) in the former case growth rate always increases with β while in the latter [3 potential], it increases but never shows tendencies to stabilize [in fact, there is a weak but steady increase in growth rate with β], (ii) a comparision of real frequencies shows qualitative as well as quantitative differences; it is interesting to note that 2 potential local calculations are closer to real frequencies of 3 potential full radius calculations.

In Fig.(3 a), we plot the electromagnetic ratio (E.M. ratio) from both local [Eq.32] and full

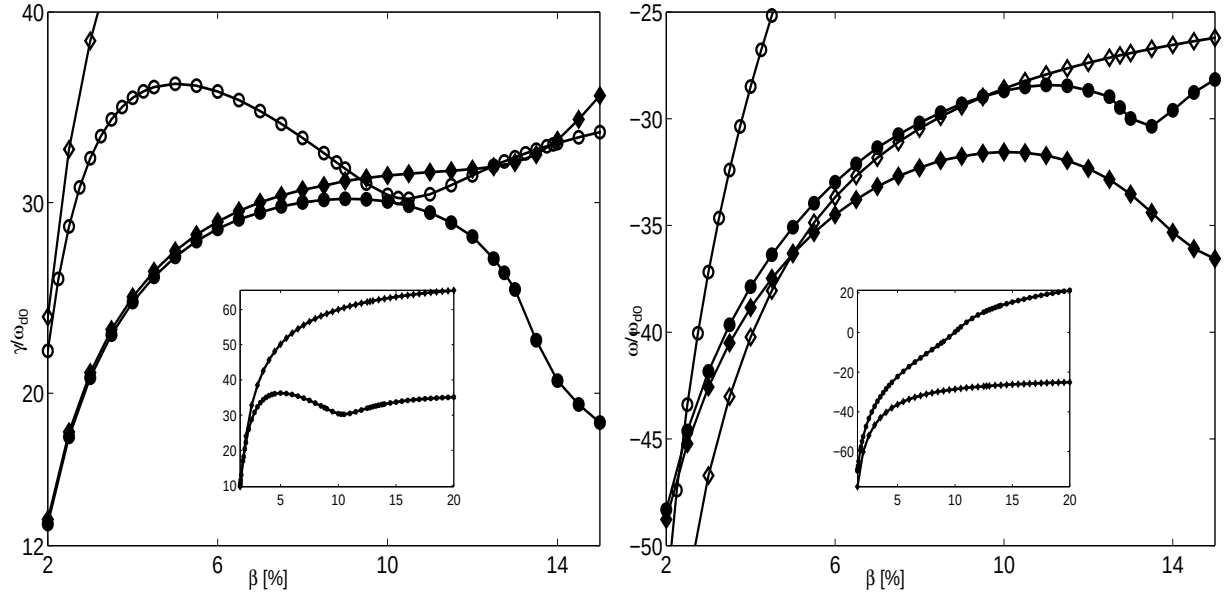

Figure 2: *Growth rates (a), frequencies (b) for profiles - I. Filled circles (filled diamonds) represent full radius results with 3 (2) potentials, while open circles (open diamonds) represent local results with 3 (2) potentials. In the inset are the complete growth rate and frequency scans from 3 and 2 potential local calculations.*

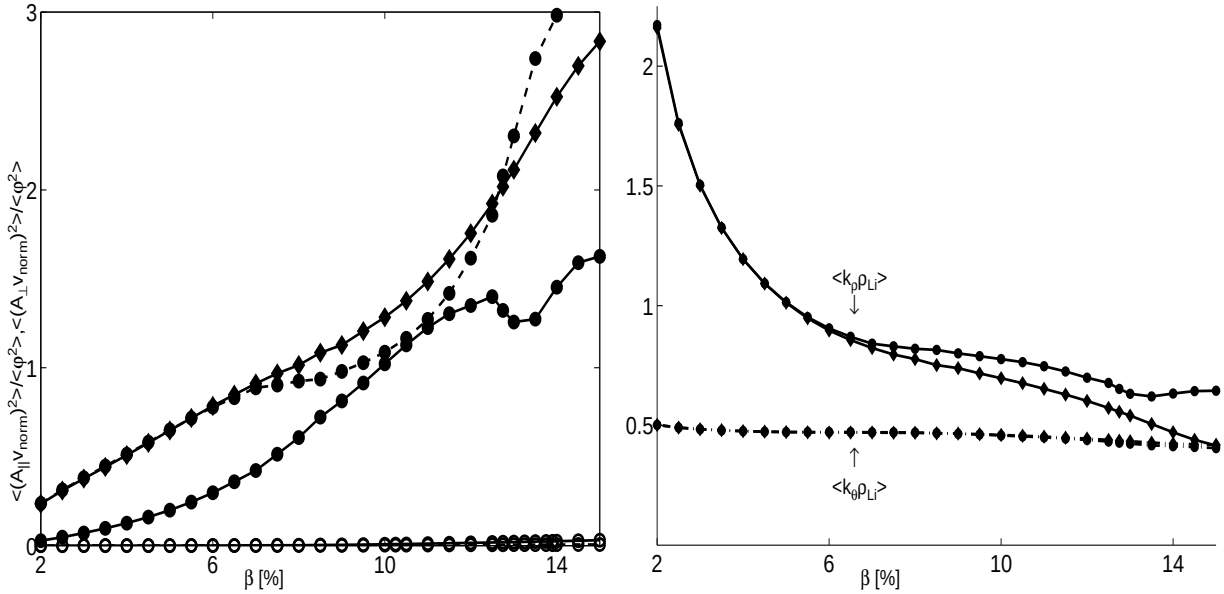

Figure 3: *(a) E.M. ratio Vs β (b) mode averaged wavenumber Vs β for profiles - I. Filled circles (filled diamonds) represent full radius results with 3 (2) potentials, while open circles represent local results with 3 potentials. In (a), dashed line with filled circle represents $A_{||}$ component computed from full radius 3-potential model.*

radius calculations [Eq.24] (Note that the results from local calculations with open circles and open diamonds lie at the bottom of the figure.) From Fig.(2a) and Fig.(3), one may divide the parameter space into 3 qualitatively different regions: (I) for $\beta < 7\%$ where $B_{||}$ fluctuations are not strong enough to have any influence on AITGs (ii) for $7\% < \beta < 13\%$ where these

fluctuations do the "turn around" of the growth rates (iii) for $\beta > 13\%$ when they have strong stabilizing tendencies on AITGs. In Figs.(4,5,6), are shown the eigenmode structures computed for 3 representative β values from each region. As can be expected, in region-(I) there are no differences between the eigenmodes with and without $B_{||}$ fluctuations of AITG mode: showing that the results of Ref.[1] obtained using only passing particles and with 2-potentials remain qualitatively unaffected in Region-I. In region-(II) & (III), there are considerable qualitative and quantitative changes. In region-II, there are two competing effects: $A_{||}$ is "more ballooning" in 3-potential results as compared to those from 2-potential analysis, (ii) electrostatic potential is radially spread out and relatively "less ballooning". In the last region (III), there is a strong stabilizing tendency due to presence of $B_{||}$ fluctuations which essentially tends to reduce the "average drift time" spent by the particles in the "bad curvature region" by rotation away from $\theta = 0$ line and mode structure is radially broadened.

For $0 < \beta < 7\%$, 2-potential $[\varphi, A_{||}]$ full radius eigenmode structures of AITG modes with only passing species was reported in Ref.[1]. In the present work, we report the mode structures for a wide range of β values (up to $\beta = 15\%$) including $B_{||}$ fluctuations with one notable difference: while ions and electrons were treated as gyrokinetic and drift kinetic respectively in Ref.[1] whereas in the present work both ions and electrons are treated as gyrokinetic. For $\beta < 7\%$ we attribute any quantitative difference in the growth rate and frequency reported in Ref.[1] and the present work to this above said feature. Again, for $\beta < 7\%$ nature of the eigenmode structure here are qualitatively same from those reported in Ref.[1]. In Fig.3 we have shown the E.M. ratio from both 2-potential and 3-potential calculations. Note that $< v_{norm} A_{||} >^2 / < \varphi >^2$ from 2-potential and 3-potential results agree very well until $\beta < 7\%$ at which point E.M. ratio $< v_{norm} A_{\perp} >^2 / < \varphi >^2$ from $B_{||}$ fluctuations becomes comparable to that of $A_{||}$ fluctuations. Thus, there are no qualitative differences between our results and those of Ref.[1] until those values of β (i.e., $\beta < 7\%$) when $B_{||}$ fluctuations become important. (See Figs.2a,4)

Full radius eigenmode structures of φ and $A_{||}$ shown in Figs.(4,5,6) have the following features in common [1]: (i) broad radial distribution arising through coupling of neighbouring flux surfaces via particle drift (ii) at radial locations of mode rational surfaces (shown in the top axis in figures showing mode resolution) where $k_{||}^m = 0$ (i.e., as if toroidal coupling is absent $n\ q(s) = m$), it is clearly seen that the corresponding poloidal mode 'dips' close to zero (due to toroidal coupling, note that $< k_{||} > \neq 0$ anywhere). This sharp radial variation around a mode rational surface demands a wide radial spectrum (i.e, κ spectrum) (iii) on these surfaces electrons behave nonadiabatic (iv) small scale structures dominate the electrostatic potential φ compared to $A_{||}$ and finally (v) $A_{||}$ component becomes more and more "ballooning" as β goes from small to larger β values: as if the poloidal "lobs" at the out-board side annihilate each other

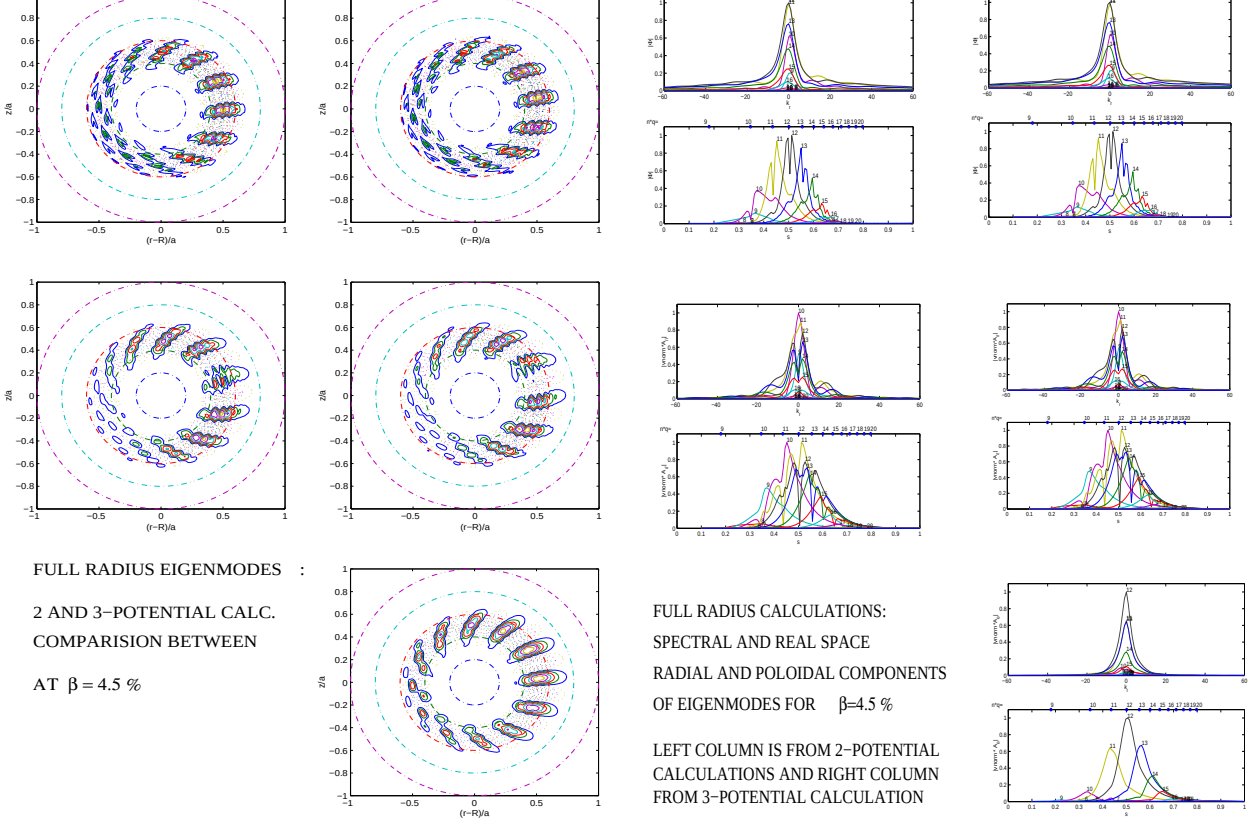

Figure 4: *Left two columns are eigenmode structures from 2 and 3-potential results and right two columns represent their poloidal and radial mode resolution. Top, middle and bottom rows are* φ, $A_{||}$, $A_{\perp}$ *respectively.* $\beta = 4.5\%$ *(see Fig.2a. for growth rate and frequency).*

(see Fig.7) such that "new lobs" are formed to keep the total number of "lobs" the same. While the above said features are common to $[\varphi, A_{||}]$ components AITG mode, $B_{||}-$fluctuations have their own signatures: (i) as can be expected, there are no sharp radial structures (mode rational surfaces are poloidal flux surfaces): thus, radial wave numbers needed to resolve the full radius eigen spectrum of $A_{\perp}$ is relatively small. (ii) $A_{\perp}$ component becomes less and less ballooning as β goes from small to large values : poloidal lobs spread out more uniformly on both in-board and out-board sides (iii) with increase in β values, $A_{\perp}$ eigenmode width "broadens" radially and at the same time rotates along poloidal direction away from $\theta = 0$ line, thus helping particles sample more of the "good curvature" on the average. Thus as a function of β, $A_{||}$ and $A_{\perp}$ behave exactly the opposite ways.

A rather important feature of a 2-dimensional (κ, k_θ) full radius calculation which treat FLR effects up to all orders is that there are no assumed *length scales* about the linear fluctuations. In fact, one can compute as a diagnostic, the eigenmode averaged $\bar{\kappa} =< \kappa >$ and $\bar{k}_\theta =< k_\theta >$ (these quantities are normalized to ϱ_{Li}) from which one can obtain some idea about dominant mode-averaged $\bar{k}_\perp =< k_\perp >$. In Fig.(3b) is shown mode-averaged wavenumbers i.e, $\bar{\kappa}, \bar{k}_\theta$ $(\bar{k}_\perp = \sqrt{\bar{\kappa}^2 + \bar{k}_\theta^2})$ as a function of β. Note that $\bar{k}_\theta$ is more or less a constant as function of

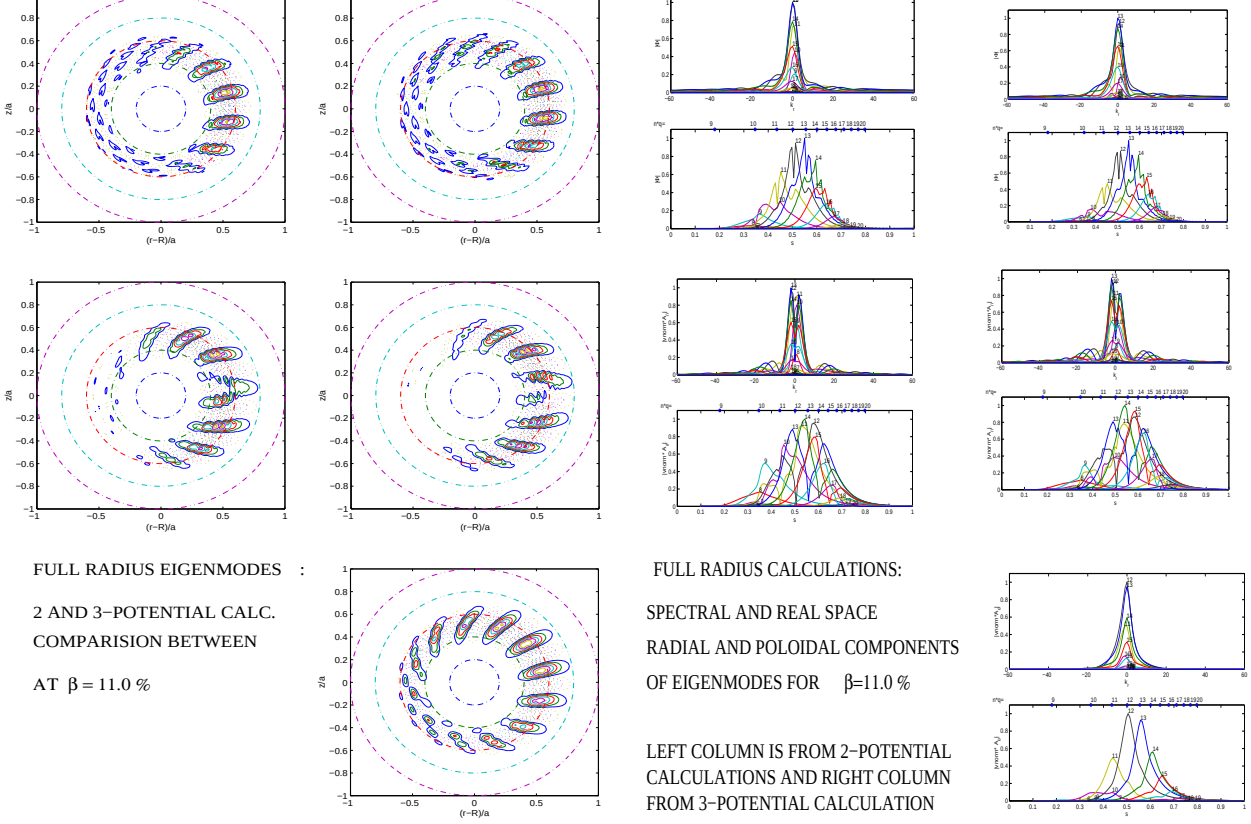

Figure 5: *Eigenmode structure and poloidal mode resolution for* $\beta = 11.0\%$ *(see Fig.2a for growth rate and frequency), symbols are as for Fig.(4)*

β. Thus $\bar{k}_\perp$ varies as $\bar{\kappa}$. For low $\beta < 4\%$, $\bar{k}_\perp > 1$, for $4\% < \beta < 10\%$, $\bar{k}_\perp \simeq 1$ and for $\beta > 10\%$, $\bar{k}_\perp \simeq 0.5$. Thus, in most parts of the parameter space, strong FLR effects are dominant. On relative terms, it implies that for cases without Shafranov shift, κ^{-1} (long radial wavelength) becomes important for large β's compared to FLR effects which are relatively less effective. Also from the mode structure of $[\varphi, A_{||}, A_\perp]$, kinetic resonances near $k_{||} \simeq 0$ surfaces which demand large κ values and spectrum are weakened by finite$-\beta$ effects. From this, one may conclude that an MHD-like (smaller absolute values of real frequency) behaviour seem to emerge at larger β values from 2-potential as well as 3-potential calculations. Nevertheless, there is an important difference: absolute values of real frequencies **increase** with increase in β (for large β) in 2-potential case making it deviate more from MHD-like, while it **decreases** with β for 3-potential case showing that AITG mode getting "closer" to acquiring MHD-like features. But note that real frequencies in both 2-potential and 3-potential cases even at large β values is still large and finite (a few times ITG frequencies at $\beta = 0$ [1]) underscoring the role of kinetic damping, transit particle harmonics even though FLR effects are steadily weakened. Hence one can conclude that presence of $B_{||}$ fluctuations stabilizes AITG mode through mode "rotation" from "bad curvature" to "good curvature" region which otherwise (i.e, without $B_{||}$) is not possible. As a remark, one may also infer from Figs.(4,5,6) and Fig.(3 c) that there

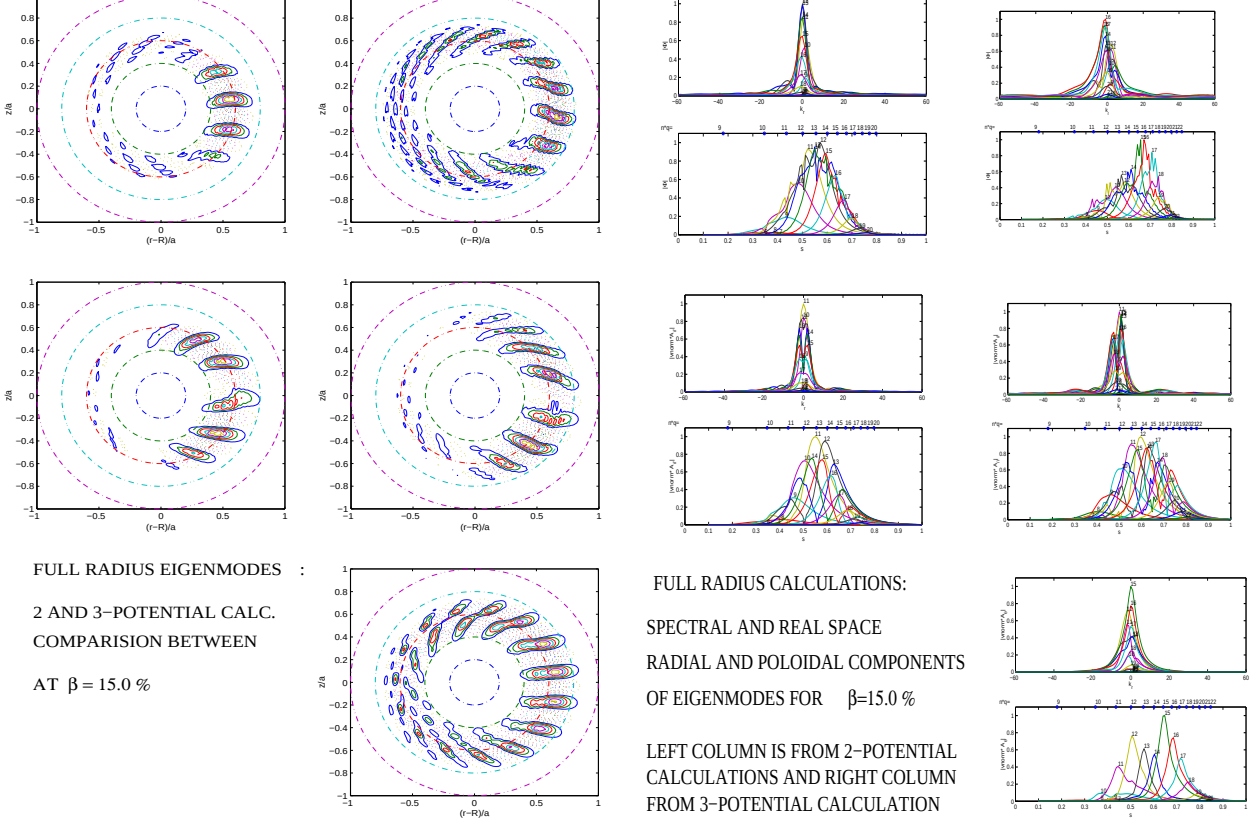

Figure 6: *Eigenmode structure and poloidal mode resolution for* $\beta = 15.0\%$ *(see Fig.2a.), symbols are as for Fig.(5)*

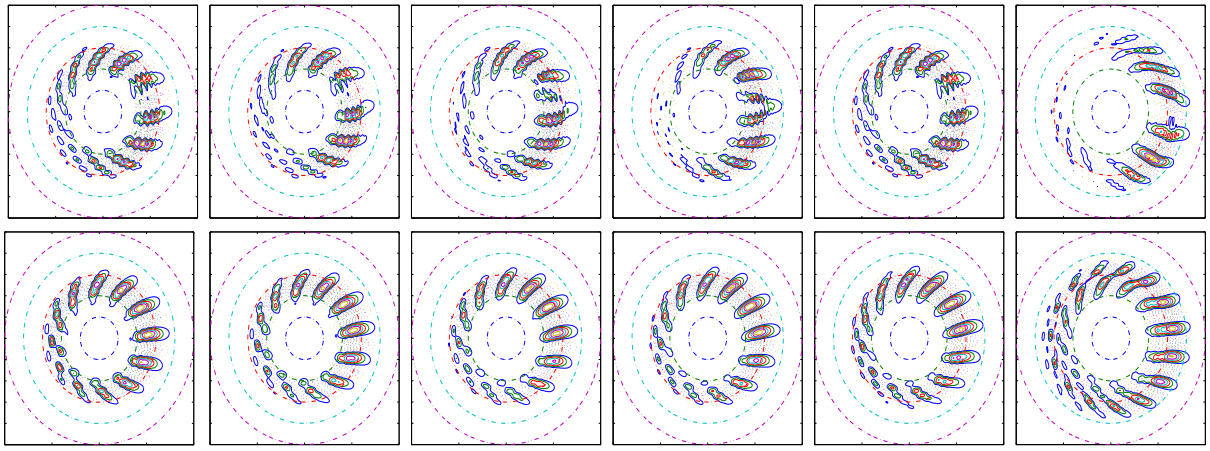

Figure 7: *Eigenmode structure* $A_{||}$ *(top row) and* $A_{\perp}$ *(bottom row) (see Fig.2a for growth rate and frequency), as a function of increasing* $\beta = 4.0,\ 6.0\ , 8.0,\ 10.0\ , 12.0$ &15.0% *along the stabilized curve in Fig.(2 a,b) demonstrating the "annihilation" of* $A_{||}$ *lobs on the outboard side "rotation" of* $A_{\perp}$ *mode to "good curvature side"*

is a good deal of radial nonlocality and consequent sampling of $q(s)$ and $\hat{s}(s)$ (which increase monotonically), a feature not captured in a standard "ballooning theory".

8.2 Shafranov shift effects on AITG mode

For demonstrating effect of Shafranov shift on the full radius eigenmodes and growth rates, we consider the following profiles and parameters.

Parameters-II:

- B-field : $B_0 = 1.0$ Tesla
- Temperature : $T_0 = T(s0) = 7.5\ KeV$
- Major Radius : $R = 2.0\ m$
- Minor Radius : $a = 0.5\ m$
- radius : $s = \rho/a\ \ 0.025 < s < 1.0$
- $\beta(s_0) = \frac{2\mu_0 N_0}{B_0^2}(T_0^e + T_0^i)$ defines N_0
- $L_{n0} = a,\ L_{T0} = 0.2\ m \rightarrow \eta(s_0) = 2.5$
- $\tau(s) = T^e(s)/T^i(s) = 1$ throughout.

Equilibrium Profiles-II:

- N-profile and T-profile
  $N(s)/N_0 = 1.0$ (Flat Density)
  $T(s)/T_0 = \exp\left(-\frac{a\ \delta s_T}{L_{T0}}\ \tanh\left(\frac{s-s_0}{\delta s_T}\right)\right)$
  $\delta s_T = 0.16$ at $s = s_0$
- q-profile & $\hat{s}$-profile:
  $q(s) = 1.01 + 1.43\ s^2 - 3.75\ s^3 + 3.82\ s^4$
  such that $q(s = s_0) = 1.21$;
  Shear $\hat{s}$ is positive and at $s = s_0,\ \hat{s} = 0.53$.

Choice of various values (above) are motivated by the following:

- From Eq.(14) it is clear that the boundary condition for the Shafranov shift [i.e., $\Delta'(\rho = 0) = 0$ has to come from the pressure gradient profile. If one were to write an expression for spatially varying density and temperature profile, we arrive at Eq.(15), whereas if one were to use constant density and varying temperature profile then one can write $\Delta'(\rho)$ as in Eq.(16). One can either have a varying $N-$profile such that $dN/d\rho = 0$ at $\rho = 0$ or have a constant density profile. Simplest choice is to have $N-$profile which is constant through out minor radius and varying $T-$profile.

- To arrive at Eq.(14), we invoked an ordering for $\Delta'(\rho) \simeq \rho$. This together with Eq.(13) derived through a perturbative approach for $\mathbf{v}_d$ implies that $\Delta'(\rho)$ has be reasonably small. That is, $\Delta'(s) \simeq \epsilon$ where $\epsilon-$is the inverse aspect ratio. For our parameters, $\epsilon = 0.25$.

- **Choice of q-profile:** Note that both Eqs.(15) and (16) depend on $q(s)$ quadratically. In order to be consistent with relatively small value of $\Delta'(\rho)$, we choose $1.01 < q(s = \rho/a) < 2.7$ such that $q(s_0) \simeq 1.21$. For these choice of parameters, $max[\Delta(s)] = \Delta(s_0) \simeq 9.2 \times 10^{-2}$ for $\beta = 2.5\%$. Hence for range of β values of our interest $[0.0 < \beta < 5.0\%]$ we have $\Delta'(s) \simeq \epsilon$ (see Fig.9)

- **Choice of shear profile:** To be able to present our results in the light of past works in finite$-\beta$ MHD ballooning modes[10, 7], shear Alfvén modes [5, 6], kinetic ballooning modes [11, 15] which employ ballooning technique but without any radial coupling (i.e., radially local) calculations, we choose monotonic magnetic shear $0.0 < \hat{s}(s) < 2.9$ such that shear at $s = s_0$ (where η peaks) is about $\hat{s}(s_0) = 0.5$.

From our results from earlier section, it is clear that AITG's are quite nonlocal modes spanning a substantial width of minor radius. Hence studies using radially local formulations may not

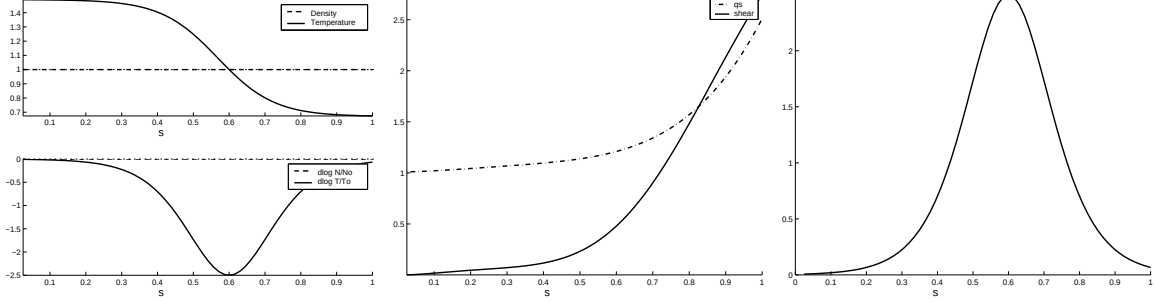

Figure 8: *Equilibrium profiles - II : Shafranov shift effect*

be adequate enough to describe them. In a tokamak, each of the following parameters viz., $\hat{s}$, $q(s)$, η, α and β vary across the region of mode localization. Consequently a single eigenmode samples a range of values of each of these "parameters". Specifically,

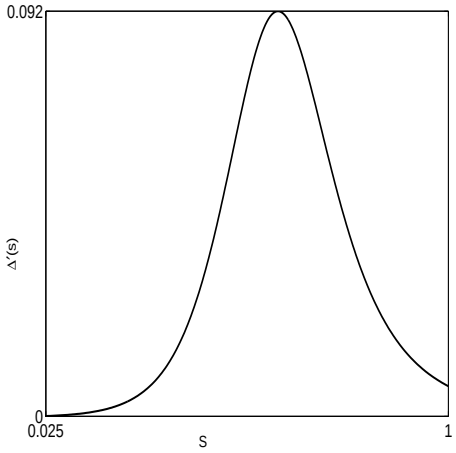

Figure 9: *Equilibrium profiles - II : A typical profile of Shafranov parameter* $\Delta'(s)$ *at* $\beta = 2.5\%$

1. Instead of a single shear value sampled by the mode at a given radial point [as in Ref.[10] for example], in present model, an entire range of equilibrium magnetic shear profile is "sampled" by a single eigenmode.

2. For each specified value of $\beta(s_0)$, present model scans an equilbrium $\Delta'(s)$ profile which peaks at $s = s_0$ and falls off away from this point. (see Fig.9). Thus unlike a standard $s - \alpha$ model, in the present model, $\beta(s)$ and $\Delta'(s)$ can be independently specified.

3. Shafranov shift is inherently a nonlocal effect. For example, in a tokamak, value of Δ' at a radial point (differential shift of a particular flux surface) is a **boundary value problem**. Meaning, imposing boundary conditions that $\Delta'(s = 0) = 0$ and $\Delta(s = 1) = 0$ completely determines a "profile" of $\Delta'(s)$ for a given equilibrium profile. While radially local ballooning calculations may be inadequate for this situation, our approach may be more suitable.

In the sections to come we will see that Shafranov shift effects further "broadens" AITG modes confirming some of the points discussed above.

We begin by first performing a "toroidal mode number (n)" scan using full radius, 2-potential $[\varphi, A_{||}]$ model including Shafranov shift to identify the most unstable mode. As result of these scans (see Fig.10) we choose toroidal mode number $n = 11$ for the rest of the results presented in this section.

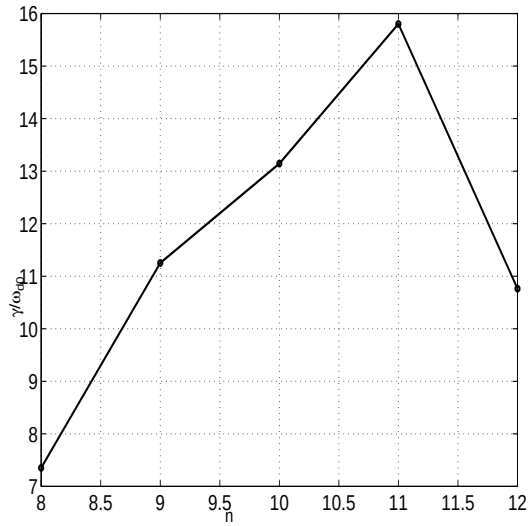

Figure 10: *Toroidal mode number ("n") scan at $\beta = 3.4\%$ of Branch-II (defined below) using 2-potential model with Shafranov shift effects.*

For $n = 11$ we scan the complex plane to identify various unstable modes. In Fig.(11), the complex plane containing the solution for profiles-II including Shafranov shift effects in 2 and 3 potential full radius calculation is shown. The same results are shown in Fig.(12 a, b) as functions of β. First, note that that for this profile (in particular, the shear values), AITG mode using 2-potential and 3-potential model without Shafranov shift effects are identical. This implies that for parameters of Profile-II $B_{||}$ fluctuations do not have any significant effect on AITG modes for $[0 < \beta < 5\%]$. In fact, we solved for β until 10% (not shown) and find no changes from 2-potential full radius results. Now, note that the maximum growth rates with Shafranov shift effects for same values of β are always less than those without [10]. In Fig.13, we compare the mode structures of Branch-I (defined below) using 3-potential model with mode structure of 2-potential model with Shafranov shift effects for $\beta = 2.5$. Also from Fig.13 it is clear that for cases with Shafranov shift effect, $B_{||}$ fluctuations do not influence the AITG mode. Therefore, we conclude that for parameters of Profile-II, $B_{||}$ fluctuations as unimportant. For the rest of this section, we study the various different mode-branches with Shafranov shift effects but using 2-potential full radius model.

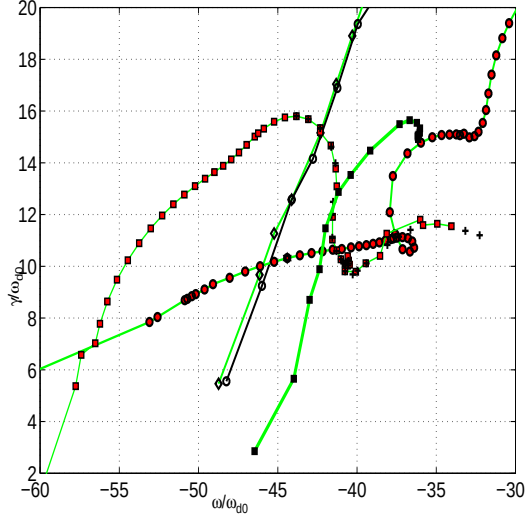

Figure 11: *For equilibrium profiles - II complex solution space: Open circle and diamonds represent 3 and 2 potential calculations with out Shafranov shift effects, filled circles represent branch-I of 2-potential solution with Shafranov shift, filled squares branch-II and filled pentagons branch-III for* $1.5\% < \beta < 4.2\%$

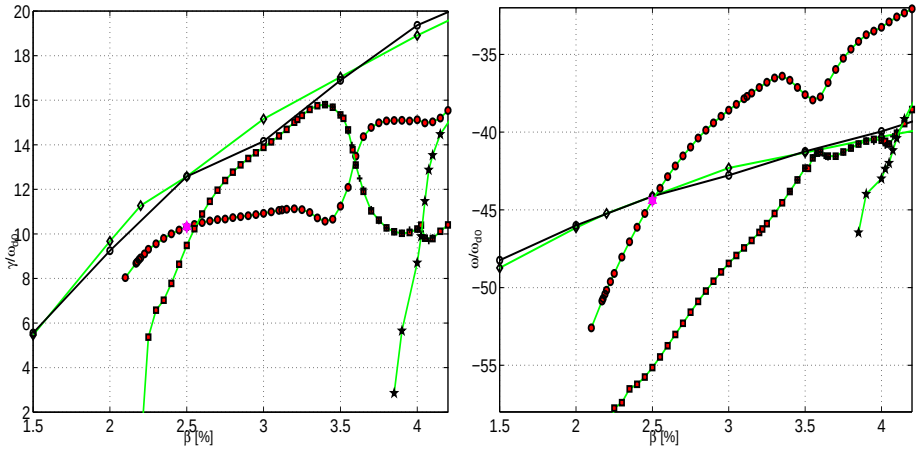

Figure 12: *Growth rate (a) and real frequencies (b) for equilibrium profiles - II: Open circle and diamonds represent 3 and 2 potential calculations with out Shafranov shift effects, filled circles represent branch-I of 2-potential solution with Shafranov shift, filled squares branch-II and filled pentgons branch-III for* $1.5\% < \beta < 4.2\%$

We find multiple eigenmodes with $anti - Sturmian$ feature, namely, the lowest growth rate modes have much more complex polodial and radial features than the highest growth rate mode. Numerically speaking, for a given resolution of equilibrium profiles, it is less demanding in terms of κ and k_θ spectrum to resolve the highest growth rate eigenmodes (and hence more accurate numerics) than otherwise.

In Fig.(12 a, b) for cases with Shafranov shift, we find 3 distinct modes. Let us label the mode with "filled circles" as Branch-I, one with "filled diamonds" as Branch-II and the one with "filled pentagons" as Branch-III respectively. Note that for $\beta \leq 2.5\%$, Branch-I is the

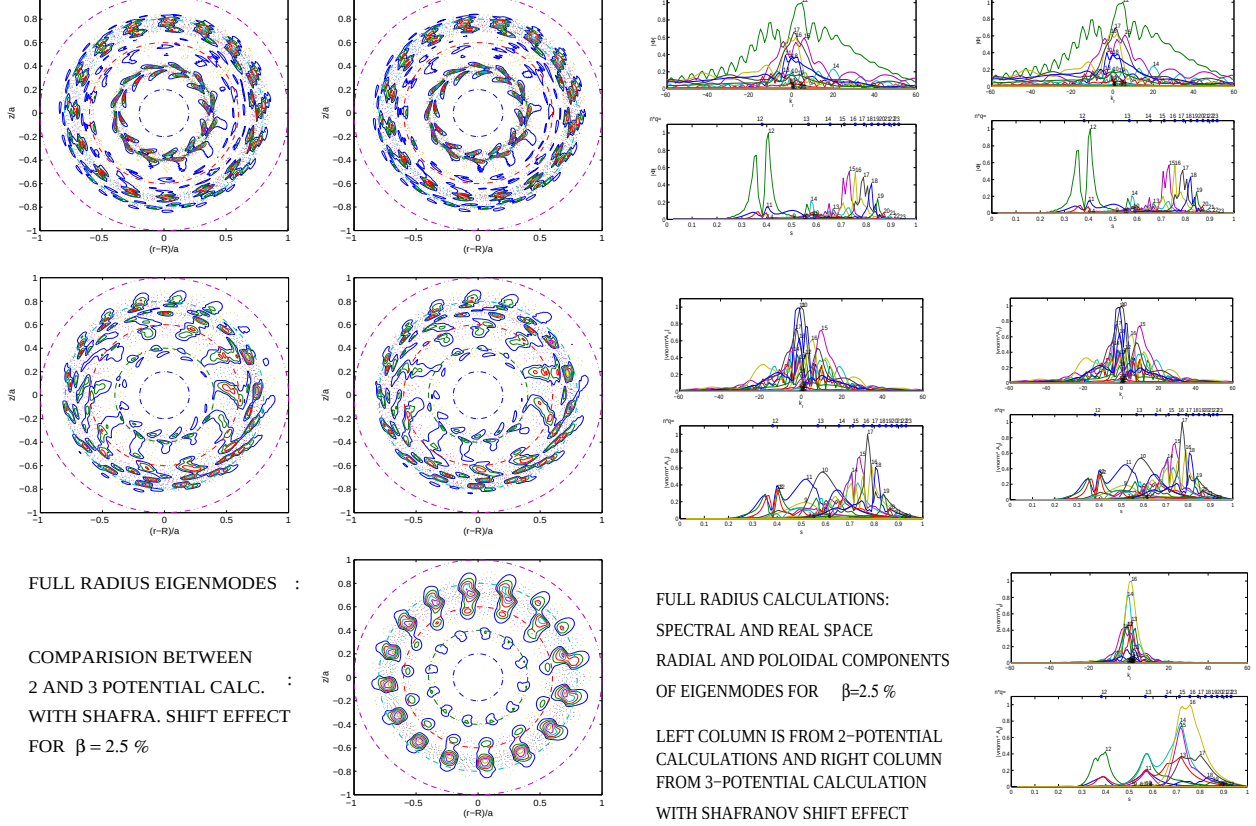

Figure 13: *Shafranov shift effects : 2-potential and 3-potential models for* $\beta = 2.5\%$. *Left two columns are mode structures and right two columns represent their poloidal and radial mode resolution. Top, middle and bottom rows are* φ, $A_{||}$, $A_{\perp}$ *respectively. Corresponding point is represented by "filled star" at* $\beta = 2.5\%$ *in Fig.12a*

highest growth rate mode. We identify this region as stability interchange region-I or SIR-I, where as for $2.5 < \beta < 3.6\%$ Branch-II is the highest growth rate mode (SIR-II) and finally, for $3.6 < \beta < 4.25$ again Branch-I has the highest growth rate (SIR-III). A new mode, Branch-III starts to become unstable for $\beta > 3.7\%$. For $\beta > 4\%$, Branch-III has higher growth rate than Branch-II. In real frequency, while Branch-I and Branch-II have distinct real frequencies for all considered values of β, but frequencies of Branch-II and Branch-III are close for $\beta > 4\%$. Anti-Sturm nature of the modes together with close real frequencies makes identifying Branch-II & III for $\beta > 4\%$ a rather tedious issue numerically. In Fig.14, we have shown the eigenmode averaged electromagnetic (E.M.) ratio and wavenumbers as function of β. Even though E.M. ratio is always greater than unity demonstrating the finite$-\beta$ character of AITG modes, note that both modes branch-I and branch-II show an increase in their E.M. ratio around SIR-II. The corresponding mode-averaged wave numbers show that while $< k_\theta >$ is nearly a constant as a function of β but $< \kappa >$ (and hence $< k_\perp >$) varies between 1 and 2 with non-monotonic behaviour. It is of interest to note that at each point of stability interchange, κ shows a change in their functional dependency on β. Also, interestingly, frequency as a function of β acquires "non-monotonic" behaviour in the region of stability change i.e., around $3.5\% \leq \beta \leq 3.65\%$

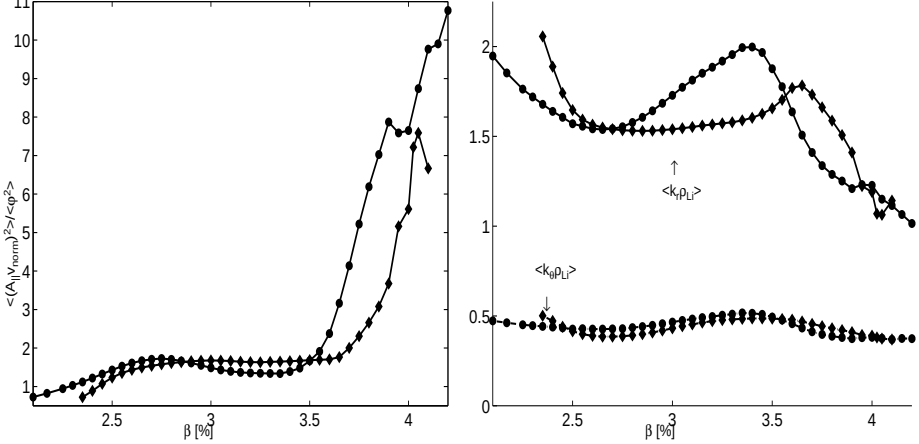

Figure 14: *E.M.ratio (left) and Mode averaged wavenumbers (right) for equilibrium profiles - II with Shafranov shift effects: filled circles represent branch-I of 2-potential model and filled squares branch-II (Branch-III is not shown) for* $1.5\% < \beta < 4.2\%$

but not around the first stability interchange region.

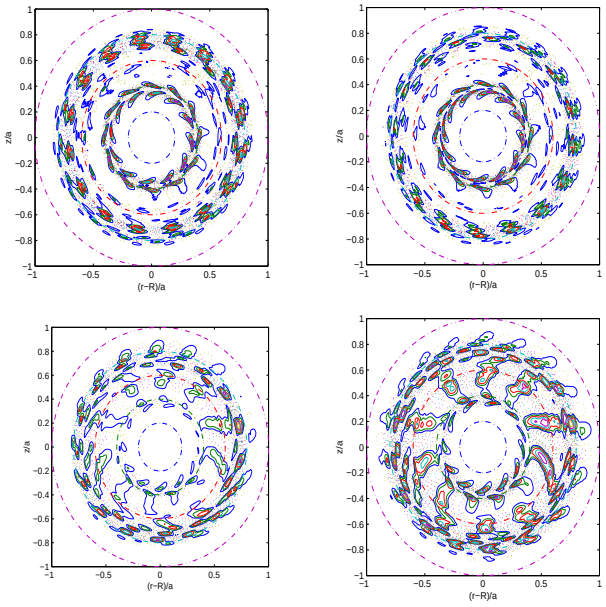

Figure 15: *Shafranov shift effect : For* $\beta = 2.35\%$ *in* stability interchange regions-*I Top row is* φ *and bottom row is* $A_{||}$ *respectively. (see Fig.12a. for growth rate and frequency).*

An interesting off-shoot of our results is that though Shafranov shift appears to bring down the growth rate of AITG modes as compared to case without Shafranov shift, for parameters of Profile-II, it appears that at least for the case of constant density profile and shear values $0.0 < \hat{s} < 2.9$, Shafranov shift alone is not sufficient to stabilize all the different modes. In fact, it appears that at any given β value, there exist multiple modes and when β is increased further, while a particular mode may get relatively stable (i.e., attain lower growth rate), yet another mode becomes unstable. Thus for no value of β studied $[0 < \beta < 4.2\%]$ do we find

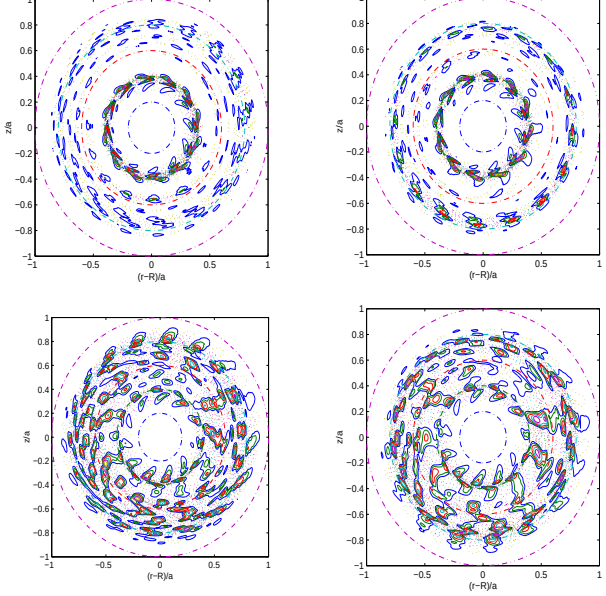

Figure 16: *Shafranov shift effect : For* $\beta = 3.4\%$ *in* stability interchange regions-*II Top row is* φ *and bottom row is* $A_{||}$ *respectively. (see Fig.12a. for growth rate and frequency).*

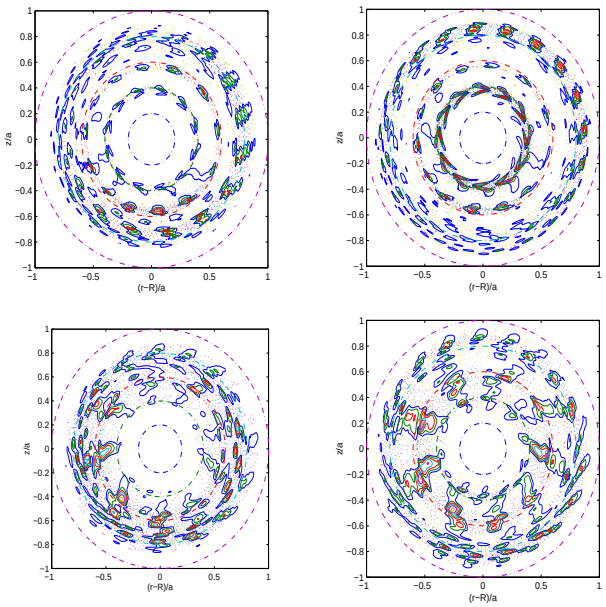

Figure 17: *Shafranov shift effect : For* $\beta = 3.85\%$ *in* stability interchange regions-*III Top row is* φ *and bottom row is* $A_{||}$ *respectively. (see Fig.12a. for growth rate and frequency).*

complete stability.

9 Conclusion

As pointed out in the Introduction, in the past AITG or KBM's modes have been addressed with varying degree of complexity. Before drawing conclusions, here we quickly summarize the basic models in the past and their results:

- $B_{||}$ fluctuations are taken into account in radially local calculations of Ref.[12] and Ref.[11] But these studies are mostly for values of β where $B_{||}$ fluctuations may not be effective.

- Finite β MHD ballooning modes (i.e., AITG/KBM without kinetic effects) were studied in Ref.[10] using radially local ballooning mode theory. Magnetic shear $\hat{s}$ was used as parameter while Shafranov shift effects were studied through variation of pressure gradient parameter [G of Ref.[10]]. Basic results are: (i) For very low positive shear values ($\hat{s} \leq 0.2$) there are no unstable MHD ballooning modes. (ii) For a given positive value of shear ($0.4 < \hat{s} \leq 1.5$), growth rate of these modes first increase and then completely stabilize with increasing pressure gradient parameter (G). (ii) Though, for large shear values, the magnitude of maximum growth rate increases, ultimately complete stability is attained. $s - \alpha$ second stability region for MHD Ballooning modes is identified.

- AITG or KBM's including kinetic effects with ballooning formalism (again, radially local) but for circular as well as non-circular flux surface were studied in Ref.[12]. Irrespective of shaping of flux surfaces, Shafranov shift effects were shown to be stabilizing. This work includes trapped electrons.

- Gyro-kinetic study with 2-potentials [φ, $A_{||}$], using ballooning formalism in standard $s-\alpha$ frame work was studied in Refs.[11]. Parametric study of varying shear $\hat{s}$, k_θ, α and η values were reported (all quantities appropriately normalized). Main conclusions are (i) for a given k_θ, η and pressure gradient length scale, growth rate increases with α or β and real frequencies decreases in magnitude (ii) for $k_\theta \simeq 1$ and $\eta \geq 2.0$, it shown that with increasing α (or β) growth rate first increases and then turns around. (iii) with increasing k_θ, again growth rate has a maximum and then stabilizes, whereas absolute value of real frequency increases (iv) increasing positive shear has stabilizing effect (for $k_\theta = 0.4$ complete stabilization is shown for $\hat{s} > 1.4$

- In Ref.[15], Shafranov shift is neglected though the model is claimed to be full radius.

- In Ref.[1], though Shafranov shift is included, it appears that the results are too sensitive to the value of $\Delta'(s)$: for a small percent [say, 5%] of the actual shift value, AITG modes are shown to be completely stabilized.

There are some basic differences between our model and those works mentioned above:

1. $B_{||}$ fluctuations couple to full radius AITGs [1] only for large positive shear. Irrespective of values of β, they seem to be completely ineffective when shear values are positive but low.

2. For large shear, $B_{||}$ fluctuations show benign effect on AITG's for large β values, i.e., for $\beta > 7\%$. Stabilization is brought about by rotation of the mode such that, inspite of strong "ballooning" tendencies of $A_{||}$ component, mode rotation induced by $B_{||}$ component reduces the "average bad curvature" felt by the particles (see Fig.7).

3. In general, AITG mode exihibits a broad eigenmode structure (mode width). Coupling of flux surfaces having different magnetic shear values (i.e., a profile of $\hat{s}$) by radial particle drifts makes the mode nonlocal. Thus a parametric magnetic shear scan model could completely be misleading.

4. Instead of a single shear value sampled by the mode at a given radial point (as in Ref.[10, 11, 12]), in our model, an entire range of equilibrium magnetic shear profile is "sampled" by a single eigenmode (with different magnetic shear values) by radially drifting particles.

5. For each specified value of $\beta(s_0)$, our model scans an equilbrium $\Delta'(s)$ profile which peaks at $s = s_0$ and falls off away from this point. Thus unlike a standard $s - \alpha$ model, in the present model, for a given "peak" value of $\beta(s)$ a "profile" of $\Delta'(s)$ exists.

6. Furthermore, the present model takes into account (i) FLR effects up to arbitrary order, Landau resonances, transit harmonic resonances, Shafranov shift effects and includes all three electromagnetic components $[\varphi, A_{||}, A_{\perp}]$.

7. A 2-dimensional model is more suitable to describe Shafranov shift which is a nonlocal effect. For example, in a tokamak, value of Δ' at a radial point (differential shift of a particular flux surface) is a **boundary value problem**. Radially local ballooning calculations clearly are inadequate to described Shafranov shift effects, especially so if the mode is known to be radially non-local.

8. Crucial differences from Ref.[1] : (i) for our Shafranov studies, the choice of equilibrium profiles and parameters are consistent with the ordering $\Delta'(s) \simeq \rho$ for the entire range of β values studied. (ii) higher order transit harmonic coupling is used for both electrons and ions (iii) effects depending on the sign of $\mathbf{v}_{||}$ are properly taken into account

We have formulated a full radius (global), electromagnetic, 2D spectral approach to the problem of gyrokinetic stability of finite$-\beta$ large aspect ratio tokamaks without equilibrium flows and using fully passing species alone. Model includes arbitrary order FLR effects for both species, all three components of electromagnetic perturbation, Shafranov shift effects and other kinetic effects discussed above. Our basic results are (i) depending on the value of magnetic shear, $B_{||}$ fluctuations can couple to 2-potential $[\varphi, A_{||}]$ AITG modes (ii) for a flat density profile and shear profile $[0.0 < \hat{s} < 2.9]$: (a) growth rates without Shafranov shift effects are in general higher

than those including Shafranov shift (b) multiple eigenmodes with competing growth rates are found to co-exist for all values of β studied [$0.0 < \beta < 4.2\%$] (c) it is shown that Shafranov effects alone would not be enough to completely stabilize AITGs: for any value of β there exist a mode (out of many) with relatively large nonzero growth rates. In the near future, trapped electromagnetic electrons (i.e., those which couple to $B_{||}$ fluctuations) will be incorporated and their effect on finite β AITGs, ETGs and other "high frequency" microinstabilities will be studied.

Acknowledgement : We are grateful to F. Zonca for useful discussions.
One of the authors (RG) is thankful to SIC-EPFL for allowing some exclusive hours of computing for a part of this work. Entire work was performed using MPI-Library on a cluster of 25 ES45 nodes from HP-Compaq with a Quadrics interconnect. Also, this work was partly supported by the Swiss National Science Foundation.

References

[1] G. L. Falchetto, J. Vaclavik and L. Villard, Phys. Plasmas. **10**(5), 1424 (2003)

[2] S. Brunner, M. Fivaz, T. M. Tran and J. Vaclavik, Phys. Plasmas. **5**(11), 3929 (1998)

[3] P. Terry, Rev. Mod. Phys. **72** (1), 109 (2000)

[4] A. B. Mikhailovskii, Nuclear Fusion, **13** 259 (1973)

[5] W. M. Tang, Nuclear Fusion **18** (8) 1089 (1978)

[6] W. M. Tang, J. Connor and R. J. Hastie, Nuclear Fusion, **21**, 1439 (1980)

[7] C. Z. Cheng, Phys. Fluids **25**, 1020 (1982); C. Z. Cheng, Physics Reports, **211** (1) 1-51 (1992)

[8] M. Kotschenreuther, Phys. Fluids **29** (9) 2898 (1986)

[9] A. D. Turnbull *et al*, Phys. Fluids B **5**, 546 (1993)

[10] B. Coppi, A. Ferreira, J. W.-K. Mark, J. J. Ramos, Nuclear Fusion, **96** (6) (1979)

[11] J. Q. Dong, L. Chen, F. Zonca, Nuclear Fusion, **39** (8) 1041 (1999); F. Zonca, L Chen, J. Q. Dong, R. A. Santoro, Phys. Plasma **6** (5) 1917 (1999)

[12] G. Rewoldt, W. M. Tang and M. S. Chance, Phys. Fluids **25** (3), 481 (1982)

[13] R. Marchand, W. M. Tang and G. Rewoldt, Phys. Fluids **23**, 1164 (1980)

[14] W. M. Tang and G. Rewoldt, Phys. Fluids B **5** 2452 (1993)

[15] H. Qin, W. M. Tang, G. Rewoldt, Phys. Plasmas **6** (6) 2544 (1999)

[16] S. Brunner and J. Vaclavik, Phys. Plasmas. **5**, 365 (1998)

[17] R. Ganesh *et al.* Varenna-Lausanne International Workshop on Theory of fusion plasmas, Eds J. W. Connor, O. Sauter and E. Sindoni, Societa Italiana Di Fisica, 261 (2002)

[18] P. J. Catto, W M. Tang and D. E. Baldwin, Plasma Physics **23** (7), 639 (1981)

[19] T. S. Hahm, W. W. Lee and A. Brizard, Phys. Fluids **31**(7), 1940 (1988)

[20] A. J. Brizard, Phys. Rev. Lett. **84** 5768 (2000)

[21] N. A. Krall and A. W. Trivelpiece, *Principles of Plasma Physics*, San Francisco Press, Inc, San Francisco, CA 94101-6800 (1986) pp:396-397

[22] S. Brunner, Ph.D thesis, EPFL, Switzerland, Thesis no:1701 (1997), pp:126-127

[23] W. Horton, Rev. Mod. Phys. **71** (3), 735 (1999), Eqs.(50)-(51)